PART III

ELECTRON BREMSSTRAHLUNG PRODUCED IN

THICK TARGETS AT INCIDENT ELECTRON

ENERGIES OF 0.2, 1.0, 2.0, AND 2.8 MeV

by

William E. Dance

David H. Rester

ELECTRON BREMSSTRAHLUNG PRODUCED IN

THICK TARGETS AT INCIDENT ELECTRON

ENERGIES OF 0.2, 1.0, 2.0, AND 2.8 MeV

INTRODUCTION

A systematic experimental study of thick target bremsstrahlung production was initiated under an earlier NASA contract, as a result of the lack of available bremsstrahlung data in the electron energy range around the rest mass energy, which is the region where theoretical calculations based on the Bethe-Heitler cross sections are expected to be least satisfactory. Experimental measurement of absolute intensities is of importance in the space shielding program in testing the validity of computational programs predicting the bremsstrahlung production, such as the Monte Carlo calculations of Berger and Seltzer[1], and the calculations reported by Scott.[2]

The results of earlier measurements of bremsstrahlung intensities from thick targets of Al and Fe in the energy range 0.5 to 3.0 MeV were reported in an earlier NASA report.[3] These measurements were continued in the present work to extend the incident electron energy range down to 0.2 MeV and the range of atomic numbers to include Be, Sn, and Au. In the present work intensity measurements were made on Be, Al, Fe, Sn, and Au at incident energies of 0.2, 1.0, and 2.0 MeV, and on Al, Fe, Sn, and Au at 2.8 MeV. Intensities were measured at photon emission angles ranging from 0 deg to 150 deg to the incident beam direction. Targets were of sufficient thickness in each case to stop the electrons. As some of the spectra for thick targets of Al and Fe reported earlier were remeasured in the present work for a greater degree of accuracy, the results presented in this report shall replace the overlapping data appearing in the previous reports.

EXPERIMENTAL PROCEDURE

The experimental geometry utilized in the measurement of thick target bremsstrahlung spectra was described in detail in NASA Report CR-334. The electron beam from the Van de Graaff accelerator was directed at normal incidence to the target, which was enclosed in an evacuated scattering chamber as shown in Fig. 1. The bremsstrahlung radiation produced in the target and emerging at an angle Θ was observed with a Trail and Raboy[4] anticoincidence spectrometer. For determining the electron beam current for currents in the range 10^{-11} to 10^{-9} amp the electrometer used in the earlier thick target bremsstrahlung measurements was replaced by a beam monitoring system which utilized a second scattering chamber, placed in front of the primary bremsstrahlung target chamber. Electron currents were then determined by observing with a Si(Li) detector the electrons scattered into a given solid angle by a thin VYNS film inserted into the beam as it traversed the monitor chamber. As the thickness of the film was approximately 10 $\mu g/cm^2$, energy loss in the film and spatial spread of the beam on the target in the bremsstrahlung chamber was negligible. Calibration of this monitor was carried out at current values in the 10^{-9} range using a current integrator.

The technique of removing the effect of the characteristic spectrometer response from the pulse height spectra was that utilized in the bremsstrahlung cross section work in another NASA report[5] from this laboratory. This procedure may be summarized: A given pulse height distribution was hand-smoothed (spectrum A). This smoothed distribution was then multiplied by the detector response matrix, yielding a "smeared" spectrum (spectrum B), which simulated

the distortion produced by the spectrometer. Spectrum A was divided, channel by channel, by spectrum B, thus producing a correction factor as a function of pulse height channel. The original unsmoothed pulse height distribution was then multiplied by these correction factors to obtain the corrected spectrum. Examples of the correction factors applied to the pulse height data are shown in Fig. 2. The curves shown are for the spectra of aluminum, at a bombarding energy of 1.0 MeV, at $\Theta = 20$ and 120 deg.

EXPERIMENTAL RESULTS

The experimental spectral distributions of bremsstrahlung intensity, $kdn/dkd\Omega$ (k = photon energy, n = number of photons), for values of the bombarding energy T_o of 0.2, 1.0, 2.0, and 2.8 MeV are presented in Figs. 3-22 for targets of the specified thicknesses. At each bombarding energy the target thicknesses were equal to or slightly greater than the mean range for electrons at that energy, as given by Berger and Seltzer[8]. The spectra are distributions of the external radiations emitted from the target slabs and hence include no corrections for photon attenuation in the target material.

The intensity spectra from Be, Al, Fe, Sn, and Au at 0.2 MeV bombarding energy, seen in Figs. 3-7, exhibit increasing hardness with atomic number Z for all photon angles, becoming nearly flat for Au in the region $0.5\ T_o < k < 0.75\ T_o$. Spectral hardening is also seen in going from the backward direction to the forward angles. An additional factor affecting the shape of the spectra below approximately $0.5\ T_o$ is photon attenuation in the target which is seen to increase with atomic number. In the case of the Au spectra, shown as histograms in Fig. 7, several factors complicate the removal of the spectrometer response from the pulse height spectra below about $k = 0.5\ T_o$. Superimposed on the continuous bremsstrahlung spectrum at 70 keV is the characteristic K x-ray from Au. In this region the continuous spectrum is decreasing sharply due to attenuation in the target. The spectral shape in this region is further distorted

by the sharp change in the photon absorption in Au around 80 keV due to the transition in the photoelectric absorption coefficient at the K edge. Above the K absorption edge, as the photon energy decreases, the attenuation rapidly increases. On the low energy side of the absorption edge the attenuation drops sharply. The resulting enhancement in the spectra at this energy combines with the Au K x-ray causing a broadening of the x-ray peak and an apparent detector resolution of about twice the actual resolution of 22%. As these effects all occur within an energy region considerably less than the resolution width of the detector, the detailed structure of the spectrum in this region is not accurately retrievable from the pulse height data. Thus the Au spectra at this bombarding energy are plotted as histograms to indicate the degree of uncertainty in the spectra.

Although all the forward angle spectra are similar in shape, the 60 deg spectrum shows somewhat greater attenuation in the region of the characteristic x-ray, resulting in additional uncertainty. On the other hand, in the backward direction attenuation is a less significant factor affecting the shape of this portion of the spectrum, and the contribution from the characteristic x-ray is relatively small compared to the continuous spectrum. Hence the 120 deg spectrum crosses the forward angle spectra and is higher than the forward spectra at low photon energies. Attenuation is also significant in the Sn spectra at the forward angles. However, the complexity arising from the K x-ray and the discontinuity in the photoelectric absorption coefficient is absent, since these effects occur in the energy region below the instrumental cut-off.

At 1.0 MeV bombarding energy intensity spectra are shown for Be, Al, Fe, Sn, and Au in Figs. 8-13. For Be, Fig. 8, spectra were taken at the forward photon angles only, as the yield at the backward angles for low atomic number approaches the magnitude of the room background, thus prohibiting reasonable counting statistics. The increasing portion of the total yield emitted in the backward direction, with increasing atomic number can be observed in a comparison of the Al spectra, Fig. 9, with the Au spectra, Fig. 12. At a photon energy $k = 0.85 \, T_o$, for example, the intensity from Al is nearly three orders of magnitude lower at 150 deg than at 0 deg, while for Au the corresponding intensity at 150 deg is only one order lower than at 0 deg. For an intermediate Z material, Fe, Fig. 10, the corresponding intensity at 150 deg is two orders lower. The portion of the spectra affected by photon attenuation is seen to be smaller than at 0.2 MeV, with no substantial effect for $k > 0.2 \, T_o$.

In the higher Z materials Sn and Au at 1.0 MeV, shown in Figs. 11 and 12, in the photon energy region below approximately $0.25 \, T_o$ the spectra tend to bend over to lower intensities in going from 0 deg to 75 deg due to the increasing attenuation in the increasing slant thickness of target material as the photon angle Θ is increased. Hence the forward angle spectra cross over and fall below the backward spectra at 120 and 150 deg, where the detector observes the photons emitted from the incident face of the target where the attenuation is small. The effect of atomic number on the intensity spectra differential in photon energy and angle at a bombarding energy of 1.0 MeV and an emission angle of 10 deg is shown in Fig. 13.

At 2.0 MeV bombarding energy, Figs. 14-18, the forward-direction "peaking" of the intensity with increasing T_o becomes apparent in the differential

spectra when these spectra are compared with the spectra at 0.2 and 1.0 MeV. For Al at T_0 = 2.0 MeV for example, the intensity at 0 deg and k = 0.5 T_0 is approximately three orders of magnitude greater than at 150 deg, whereas for Al at 0.2 MeV the intensity at 0 deg, k = 0.5 T_0, is only a factor of 5 greater than that at 150 deg. For low atomic numbers this effect becomes more pronounced with increasing photon energy, as the spectra fall off toward the high energy end more rapidly as the emission angle is increased. By comparing the same spectra from Al (Z = 13) at k = 0.85 T_0, it is seen that the 0 deg intensity at T_0 = 2.0 MeV is nearly five orders of magnitude greater than the 150 deg intensity, while at T_0 = 0.2 MeV the 0 deg intensity is only a factor of 20 greater than the 150 deg intensity at that photon energy.

The intensity measurements at 2.8 MeV bombarding energy for Al, Fe, Sn, and Au are shown in Figs. 19-22. Spectra are given for the forward direction only for Sn and Au, as at this energy the radiation is most peaked in this direction and the low yield-to-background ratio at backward angles again prohibited the gaining of meaningful data at these angles.

The measured bremsstrahlung intensity distributions at each bombarding energy, kdn/dkdΩ, were integrated over the forward angles 0-90 deg and over all angles 0-180 deg. For this integration a modified Simpson's rule, which utilizes unequal increments in the integration variable, was utilized. The results of these integrations are given for each incident electron energy as a function of atomic number in Figs. 23-30. The spectra integrated over 0-90 deg are generally similar in shape to the differential spectra observed in the region from Θ = 45 to 75 deg, as these points are weighted heavily by the sin Θ factor in the Simpson integration. At T_0 = 2.0 and 2.8 MeV comparison of

the forward angle integrations with the integrations from 0 to 180 deg show similar spectral shapes for the low Z materials, with an increasing contribution to the low energy end of the spectrum from the backward angles for higher atomic numbers, due to the absence of appreciable attenuation when the photons are observed from the incident-beam side of the target. At T_o = 0.2 MeV, however, from a similar comparison there is an appreciable contribution from the backward angles for k<0.5 T_o even for the low Z materials Al and Be.

Angular distributions of the bremsstrahlung intensities integrated over photon energy, $dI/d\Omega$, are given in Figs. 31-34. The integrations are carried out for photon energies greater than a cut-off energy which varies in these integrations with the bombarding energy. The respective cut-off energies for T_o = 0.2, 1.0, 2.0, and 2.8 MeV are 36 keV, 50 keV, 133 keV and 171 keV. The forward peaking with increasing bombarding energy of the intensity per unit solid angle is quite apparent from these distributions. The dashed lines connecting the experimental data points converge to a value of zero at 90 deg because at this angle for normal electron incidence the photon detector observes an infinite thickness of target material.

The total energy radiated from the targets was determined by integrating the spectra over photon energy and angle. The total energy radiated, as a function of electron energy and atomic number, is shown in Fig. 35. The solid lines are least squares fit to the experimental data points. From these plots the total external energy E, integrated from 0 to 180 deg may be written:

$$E_{Be} = 1.4 \times 10^{-3} T_o^{2.16}$$
$$E_{Al} = 4.6 \times 10^{-3} T_o^{2.02}$$
$$E_{Fe} = 1.0 \times 10^{-2} T_o^{1.91}$$

$$E_{Sn} = 1.6 \times 10^{-2} T_o^{2.07}$$

$$E_{Au} = 2.3 \times 10^{-2} T_o^{1.90}$$

where E is in MeV/electron and T_o is in MeV. If the Z dependence is removed from the coefficient in the above expressions the total energy may be written as:

$$E = CZT_o^A.$$

The values of C and A from the data of Fig. 37 then are given in the following table:

Z	C	A
4	3.53×10^{-4}	2.16
13	3.51×10^{-4}	2.02
26	3.85×10^{-4}	1.91
50	3.24×10^{-4}	2.07
79	2.96×10^{-4}	1.90

A detailed discussion of the experimental errors in the measurement of bremsstrahlung cross sections was given in reference 4. As the experimental geometry used in the thick target intensity measurements was essentially the same, the sources of error for the most part are those that apply to the cross section measurements. The errors in the present measurements at electron energies 1.0, 2.0, and 2.8 MeV may be summarized as follows:

(1) Electron current integration: $\pm$ 5%

(2) Detector efficiency – Solid angle factor: $\pm$ 3% for k<2.0 MeV and $\pm$ 5% for k>2.0 MeV.

(3) Electron beam energy: $\pm$ 1.5% at 1.0 and 2.0 MeV; $\pm$ 2.5% at 2.8 MeV.

(4) Errors introduced by photon angle measurement: $\pm$ 3%.

(5) Statistical fluctuations: $\pm$ 3% below 0.5 T_o for $\theta < 90$ deg;

$\pm$ 6% below 0.5 T_o for $\theta < 90$ deg; $\pm$ 5% at 0.9 T_o for $\theta = 0$ deg;

$\pm$ 30-60% above 0.9 T_o for $\theta > 30$ deg.

(6) Detector response removal: In regions where the spectral values

decrease slowly as the photon energy increases the method of

response removal is accurate to within 3%. Near the spectral

end-points the uncertainty increases to approximately 15% at 0.9 T_o

and 30 to 60% at the high energy limit. In the Sn and Au spectra

at 1.0 and 2.0 MeV, which fall off sharply at the low photon

energy end due to attenuation, additional uncertainty is introduced

into that spectral region by the method of response removal used,

since the "tail" portion of the response matrix becomes more sig-

nificant with respect to the bremsstrahlung yield, and since some

distortion results from the presence of the K x-ray. This effect

is greatest in the 1.0 MeV Au spectrum at 75 deg. The lowest

plotted point is in error possibly by as much as a factor of 2.

However, the next point, at 132 keV, has an estimated uncertainty

of 30%. At the other forward angles for gold, and at 75 deg for

Sn at 1.0 MeV incident energy the estimated error in the lowest

point (100 keV) is 20%. Also affected by this attenuation is the

2.0 MeV spectrum for Au at 75 deg for which the estimated error

in the lowest plotted point at 222 keV is 10%.

The combined error in the measurements at $T_0 = 1.0$, 2.0 and 2.8 MeV is estimated to be $\pm$ 15% for photon energies below 2 MeV in the region 0.15 T_0 to 0.9 T_0 for Z = 4, 13, and 26, and in the region 0.30 T_0 to 0.9 T_0 for Z = 50 and 79. For photon energies above 2 MeV and below 0.9 T_0 the estimated error is $\pm$ 18%. In the data at 0.2 MeV the estimated error is $\pm$ 20% for $\theta <$ 90 deg and $\pm$ 30% for $\theta >$ 90 deg.

REFERENCES

1. M. J. Berger and S. M. Seltzer, <u>Proceedings of Second Symposium on Protection Against Radiation Hazards in Space</u>, Oct. 12 - 14, 1964, NASA SP-71.

2. W. Wayne Scott, NASA TND-2659.

3. William E. Dance and Leo L. Baggerly, Part I, NASA CR-334 (Dec. 1965).

4. C. C. Trail and Sol Raboy, Rev. Sci. Instr. 30, 425 (1959).

5. D. H. Rester and W. E. Dance, NASA CR-759 (April 1967).

6. M. J. Berger and S. M. Seltzer, NASA SP-3012 (1964).
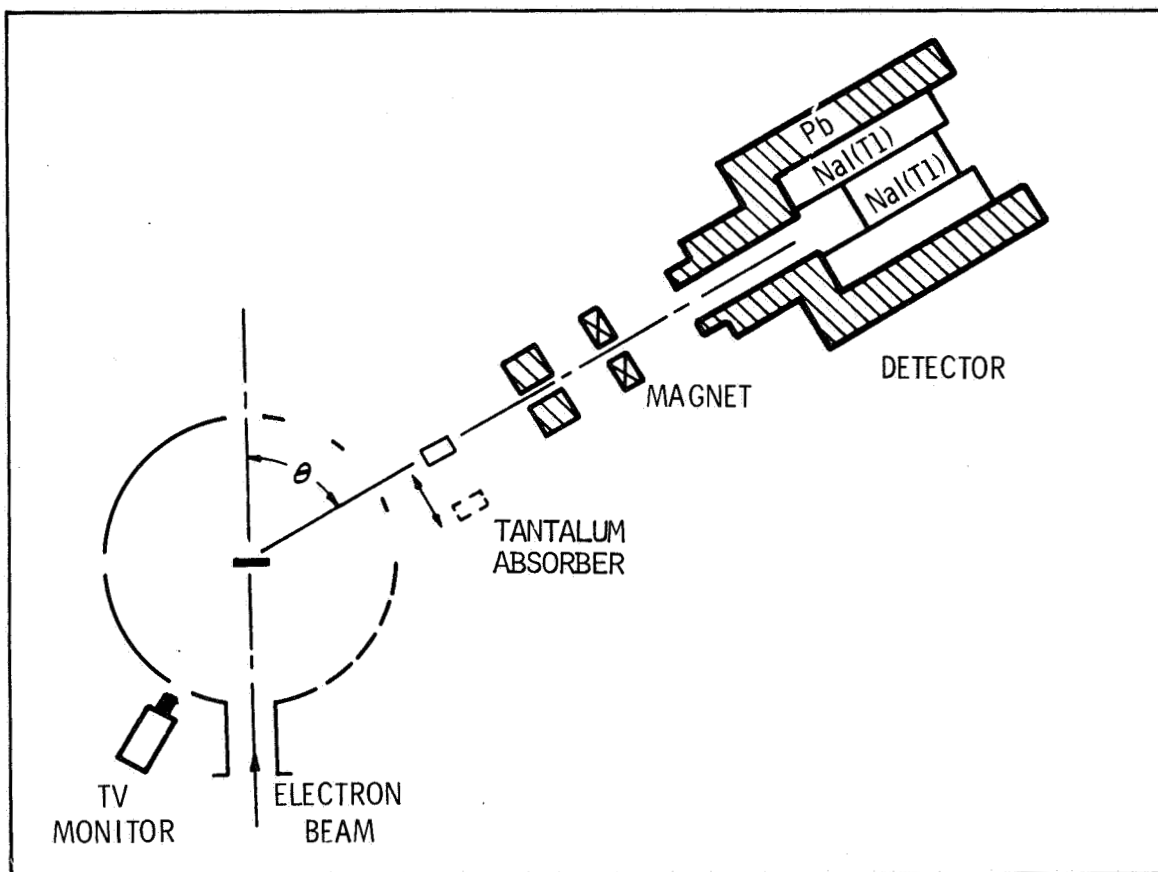
FIGURE 1. EXPERIMENTAL ARRANGEMENT OF BREMSSTRAHLUNG CHAMBER AND SPECTROMETER.
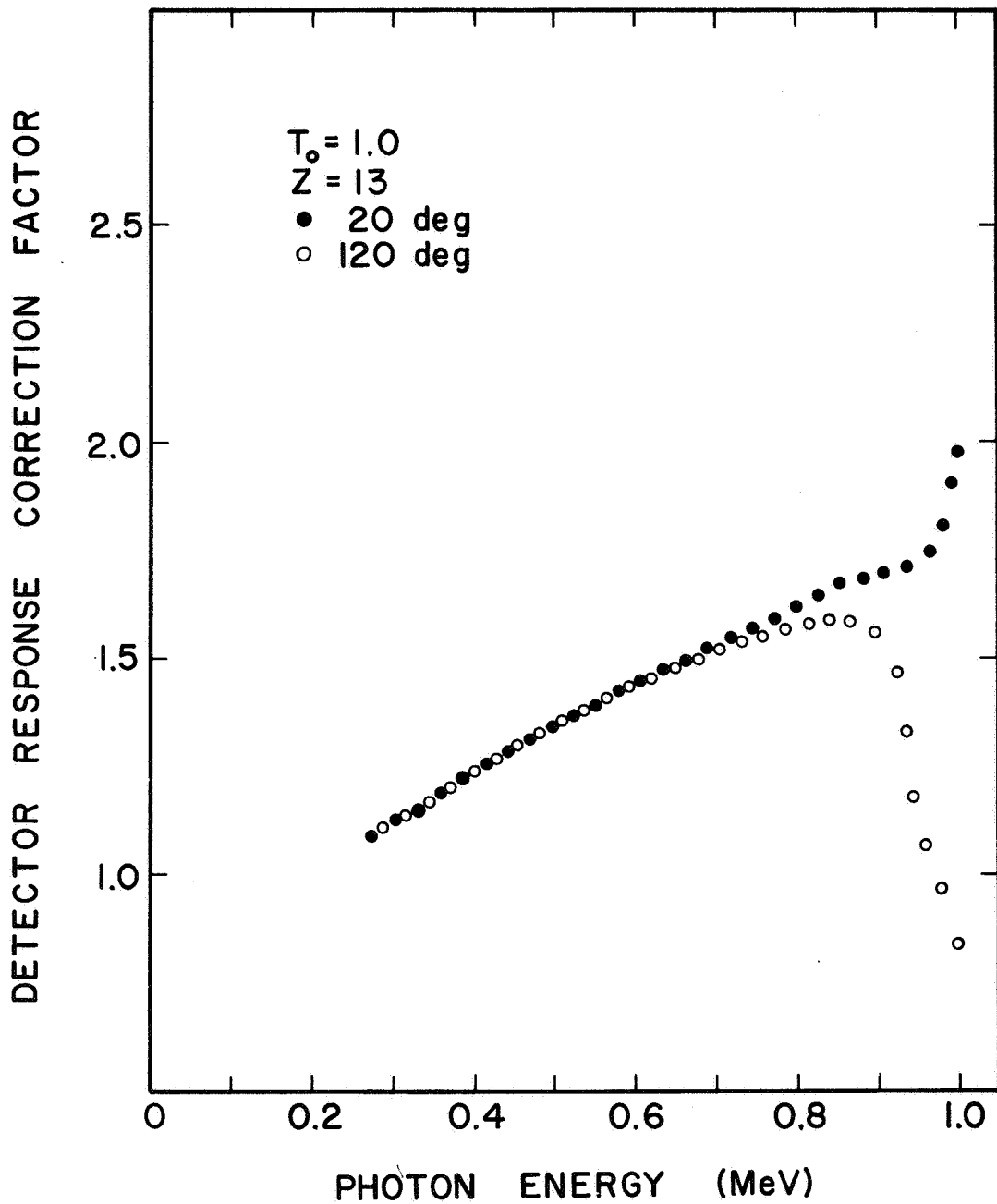
FIGURE 2.   EXAMPLES OF CORRECTION FACTORS FOR REMOVAL OF SPECTROMETER
RESPONSE FROM THE PULSE HEIGHT SPECTRA.
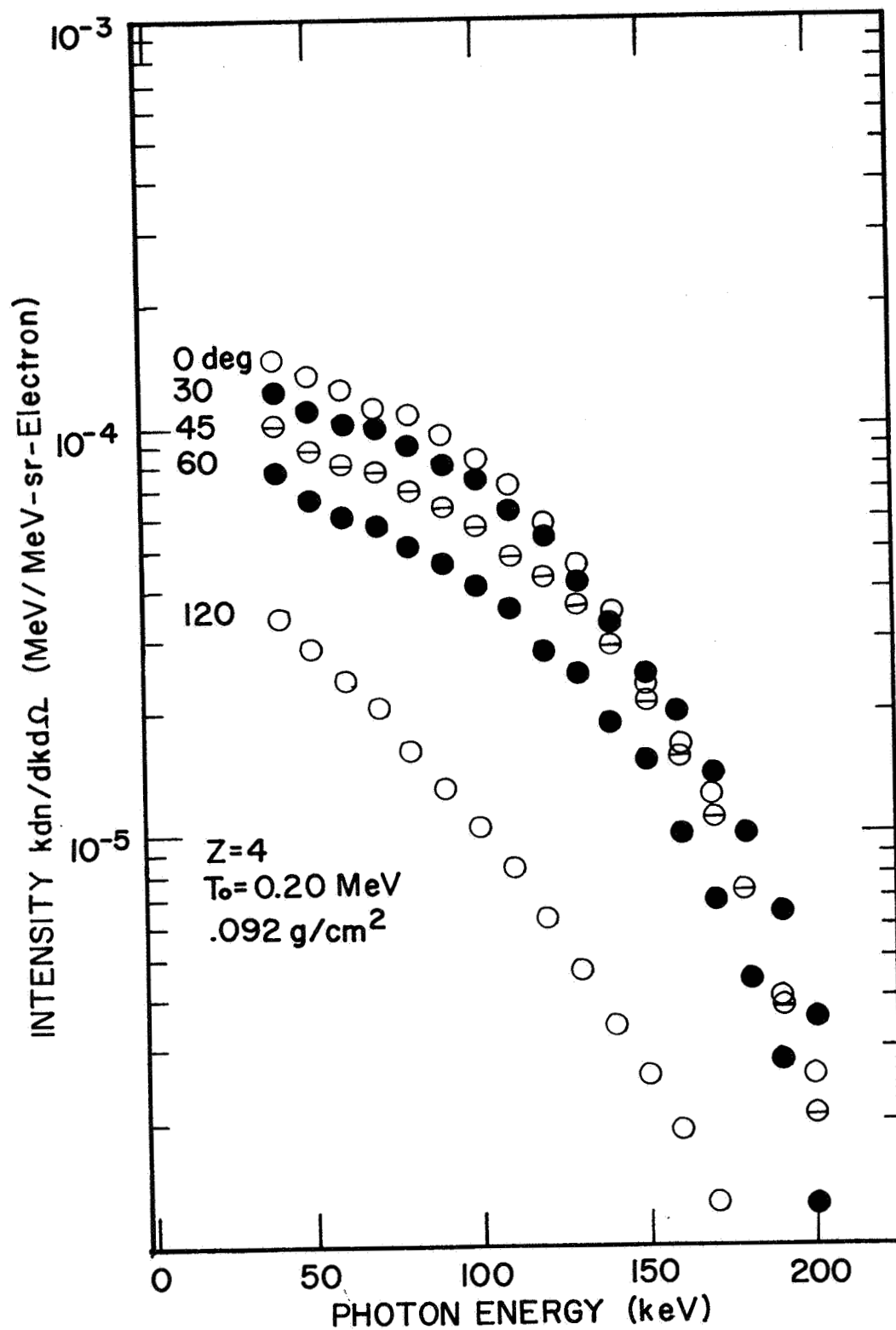
FIGURE 3.   BREMSSTRAHLUNG DIFFERENTIAL INTENSITY SPECTRA FOR 0.2 MeV
ELECTRONS ON A THICK   BE TARGET
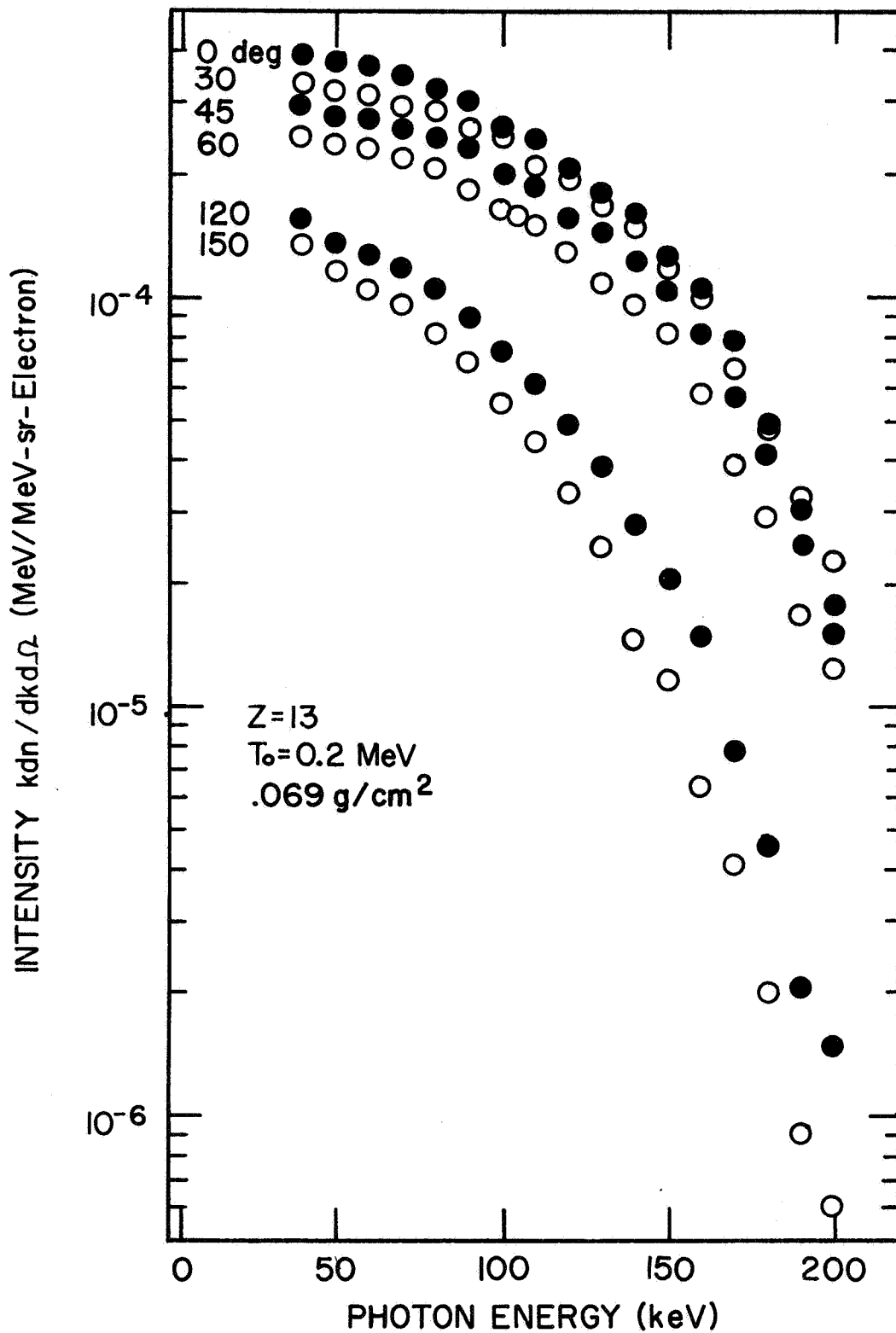
FIGURE 4.   BREMSSTRAHLUNG DIFFERENTIAL INTENSITY SPECTRA FOR 0.2 MeV
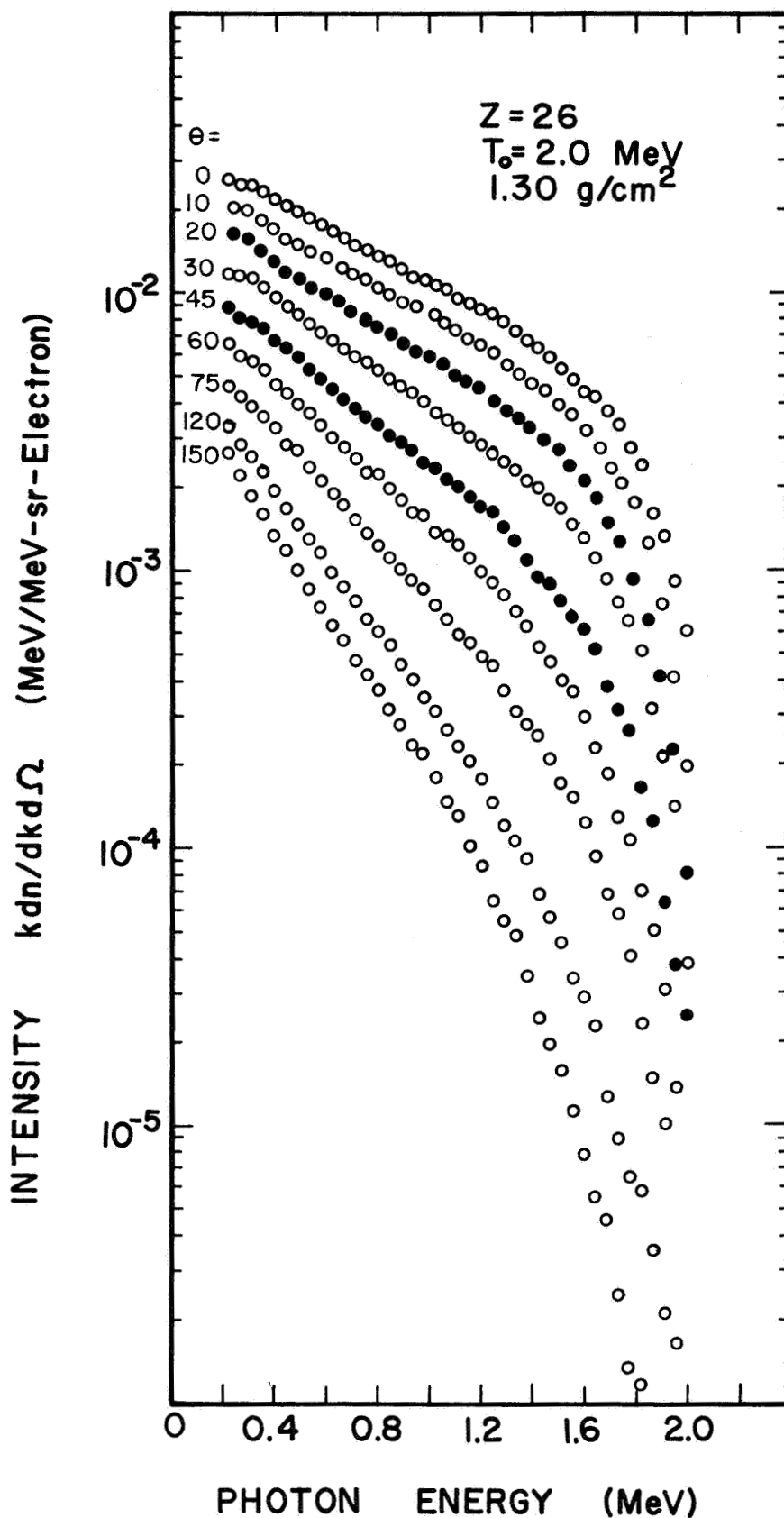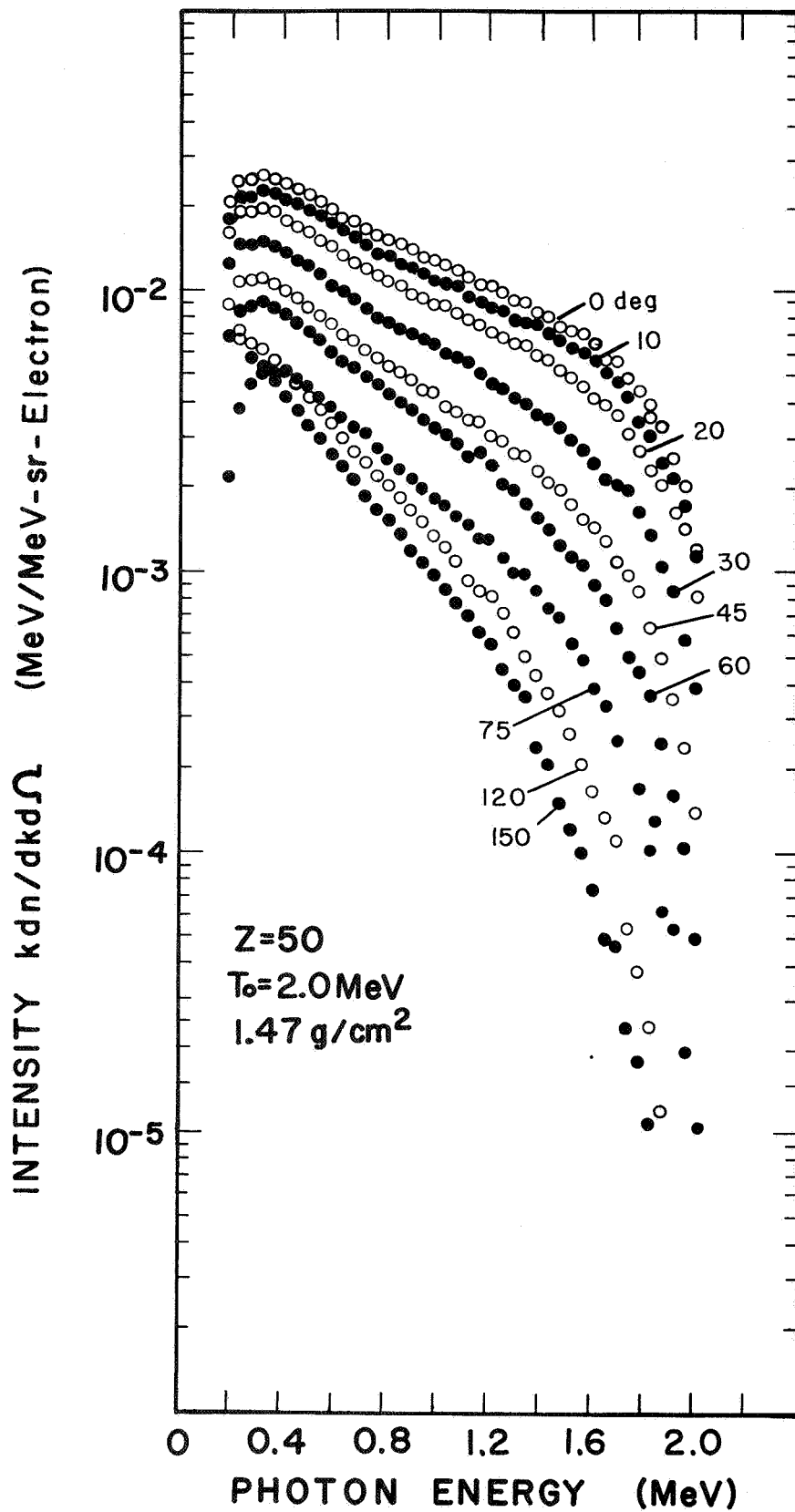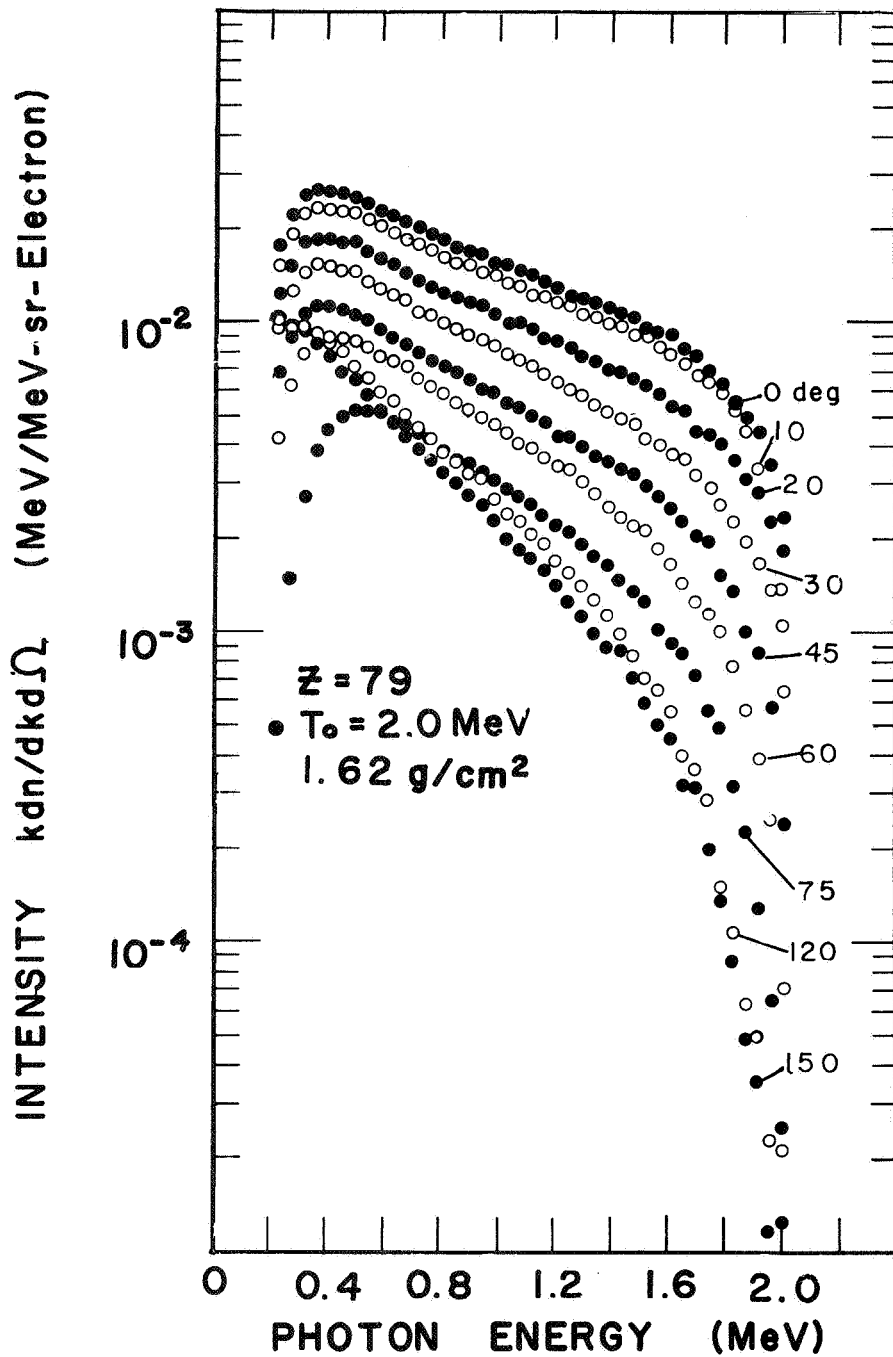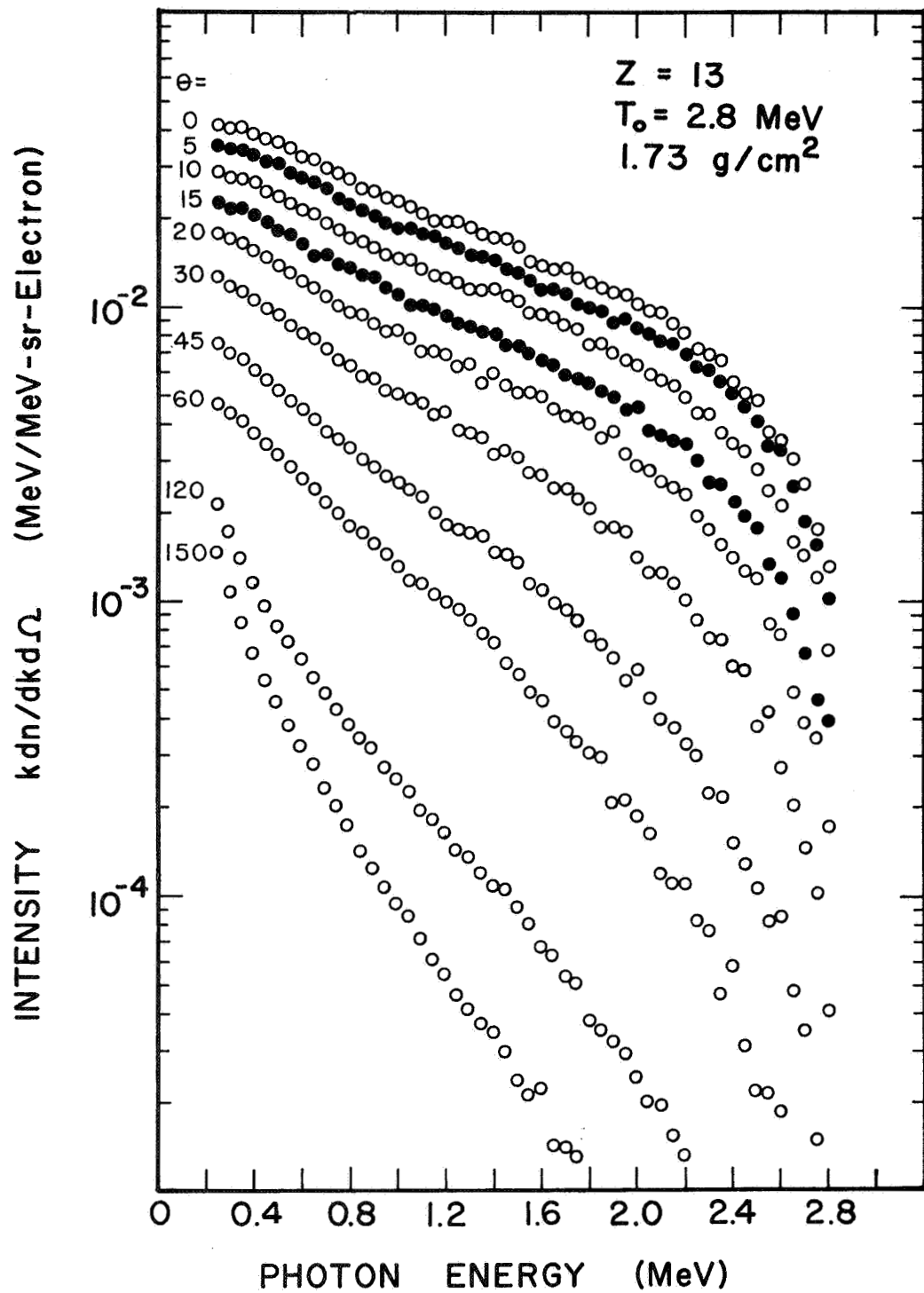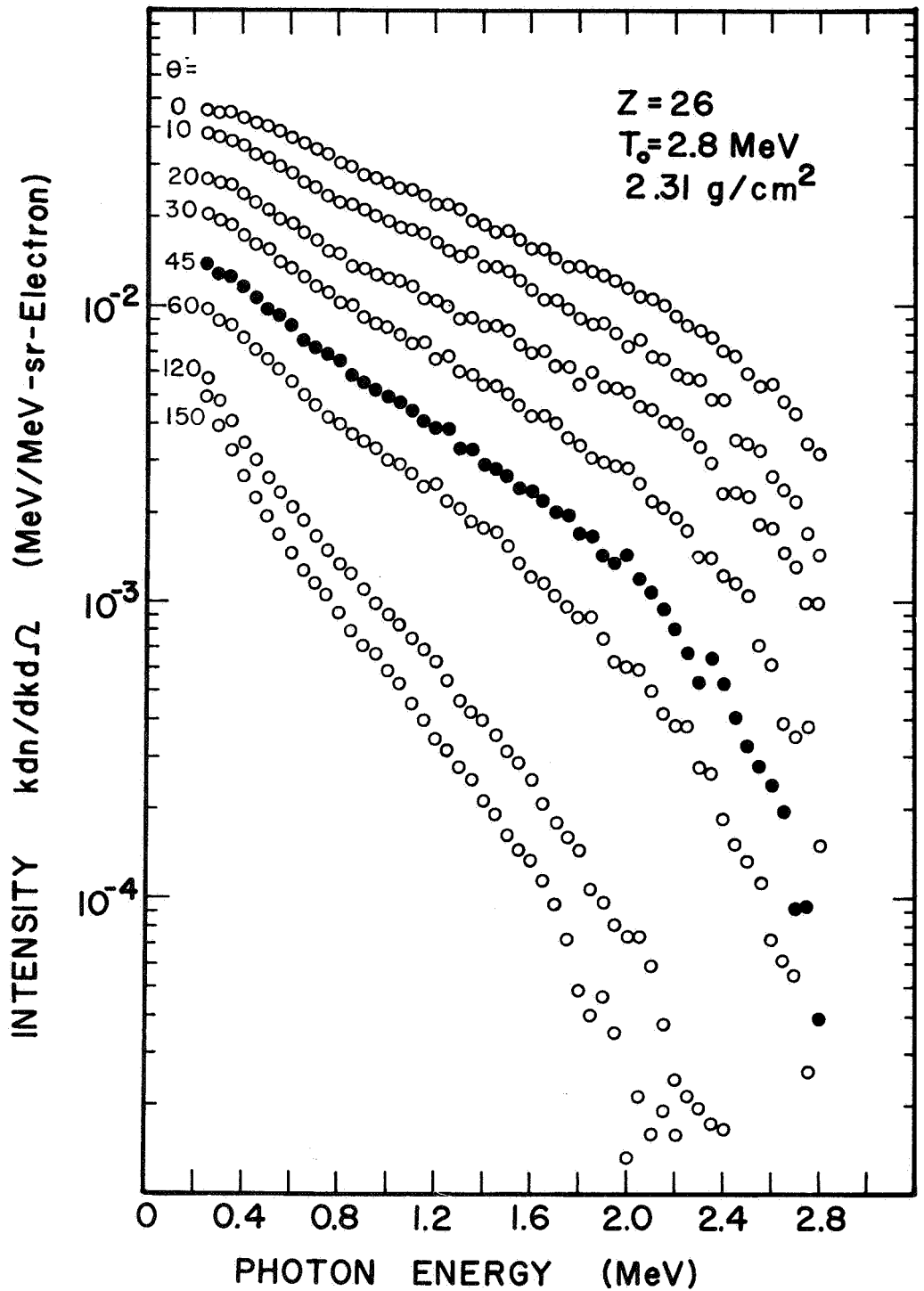ELECTRONS ON A THICK Al TARGET.
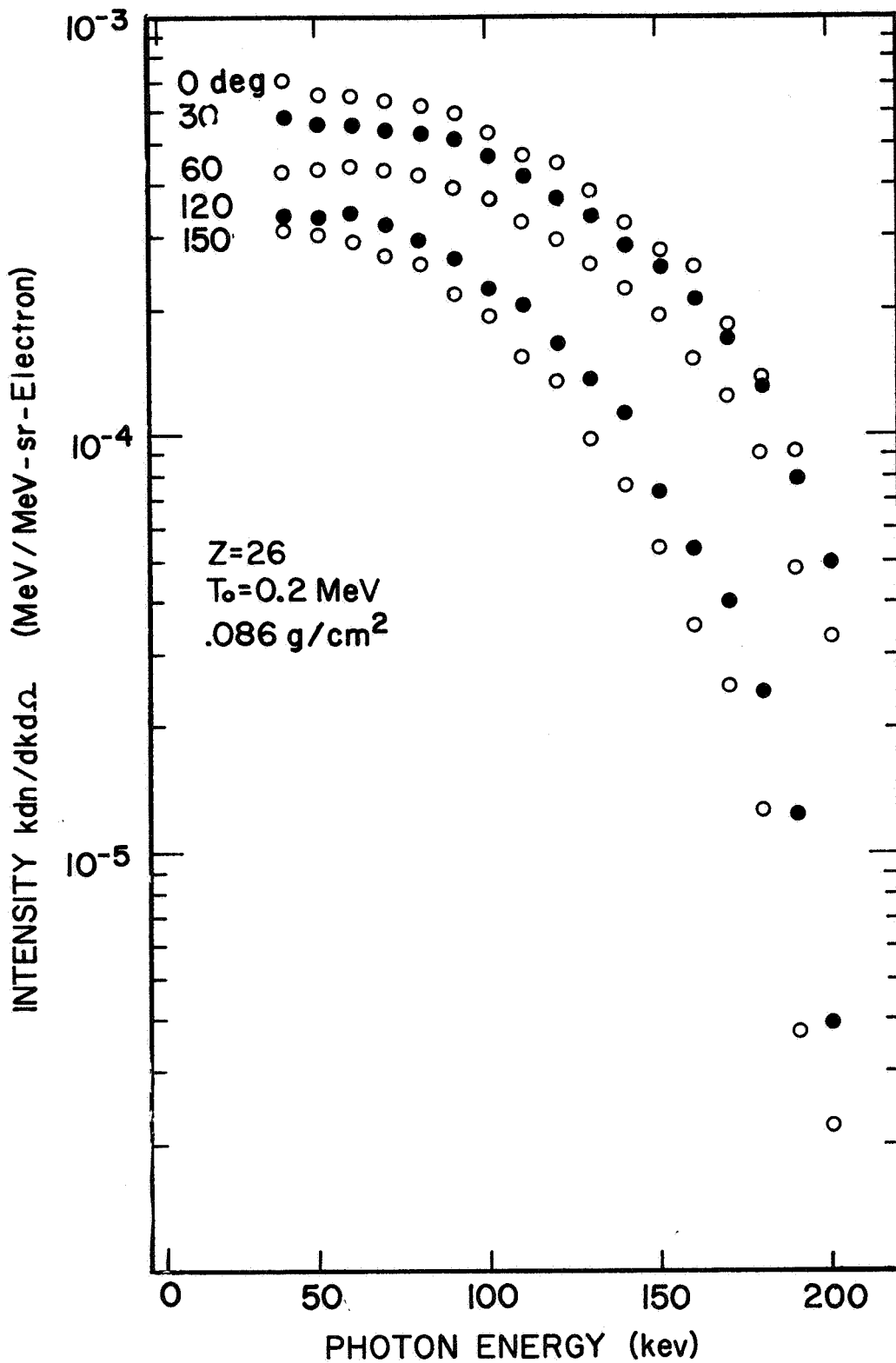
FIGURE 5.   BREMSSTRAHLUNG DIFFERENTIAL INTENSITY SPECTRA FOR 0.2 MeV
ELECTRONS ON A THICK Fe TARGET.
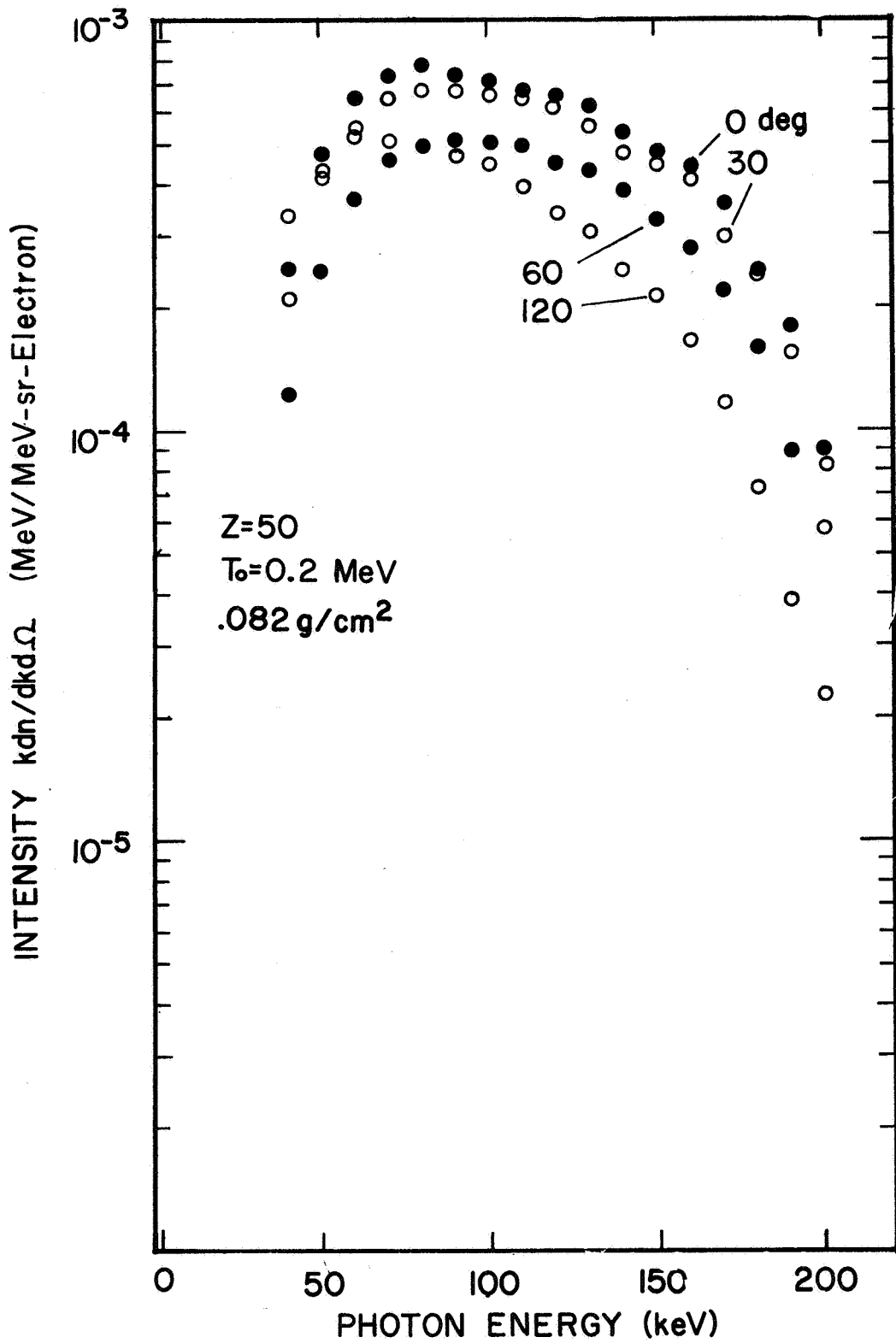
FIGURE 6.   BREMSSTRAHLUNG DIFFERENTIAL INTENSITY SPECTRA FOR 0.2 MeV
ELECTRONS ON A THICK Sn TARGET.
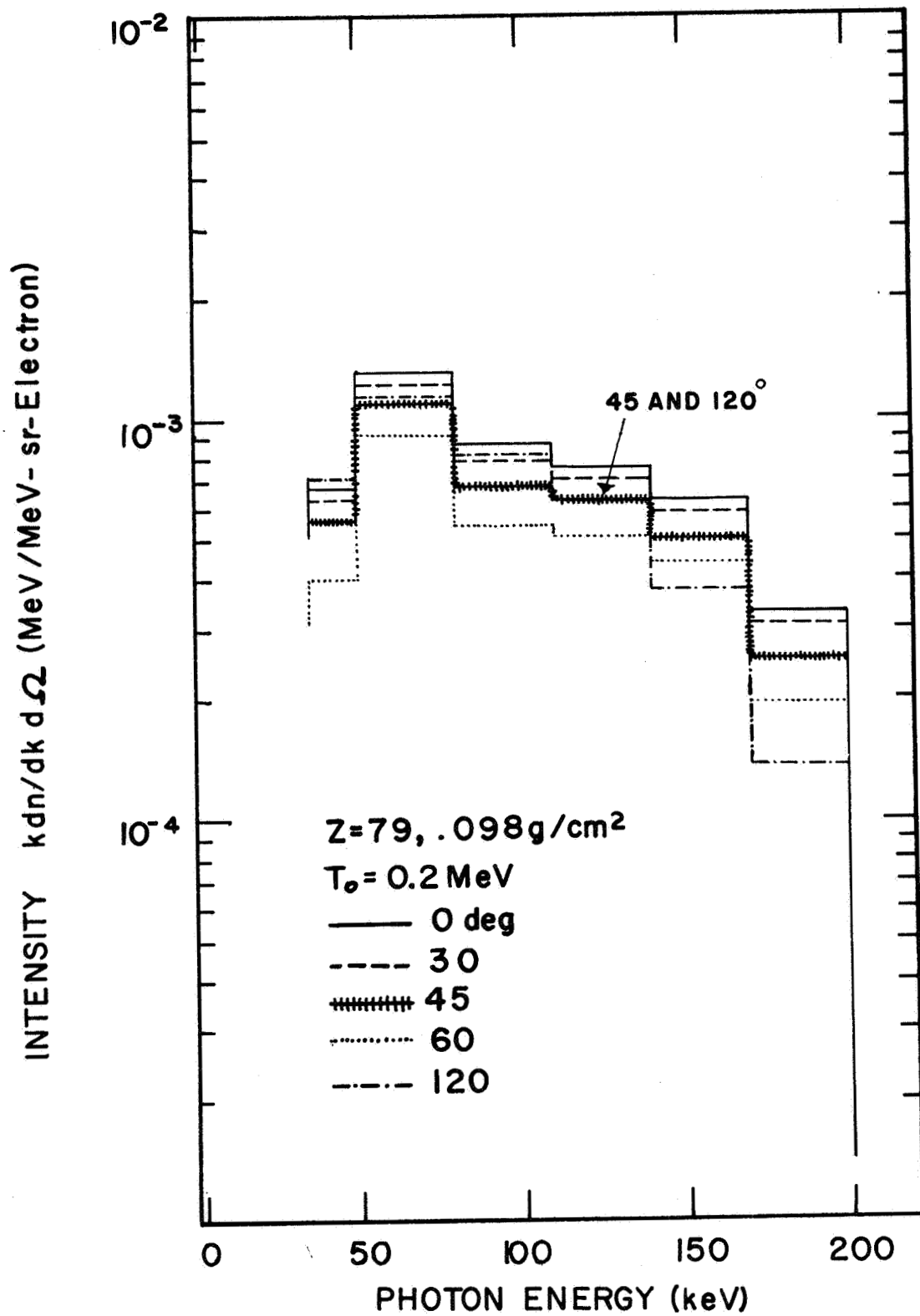
FIGURE 7. BREMSSTRAHLUNG DIFFERENTIAL INTENSITY SPECTRA FOR 0.2 MeV
ELECTRONS ON A THICK Au TARGET.

-302-
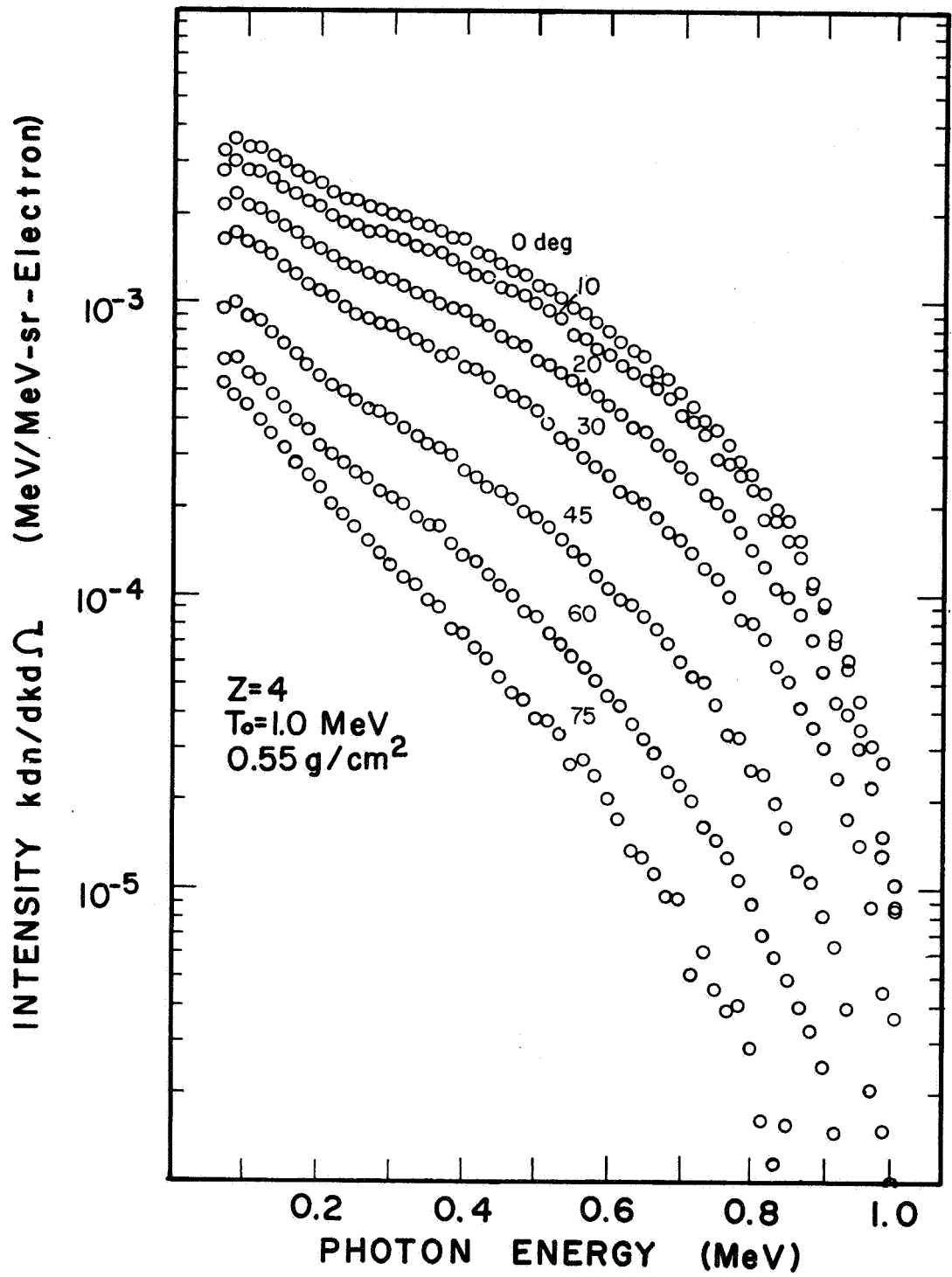
FIGURE 8. BREMSSTRAHLUNG DIFFERENTIAL INTENSITY SPECTRA FOR 1.0 MeV
ELECTRONS ON A THICK Be TARGET.
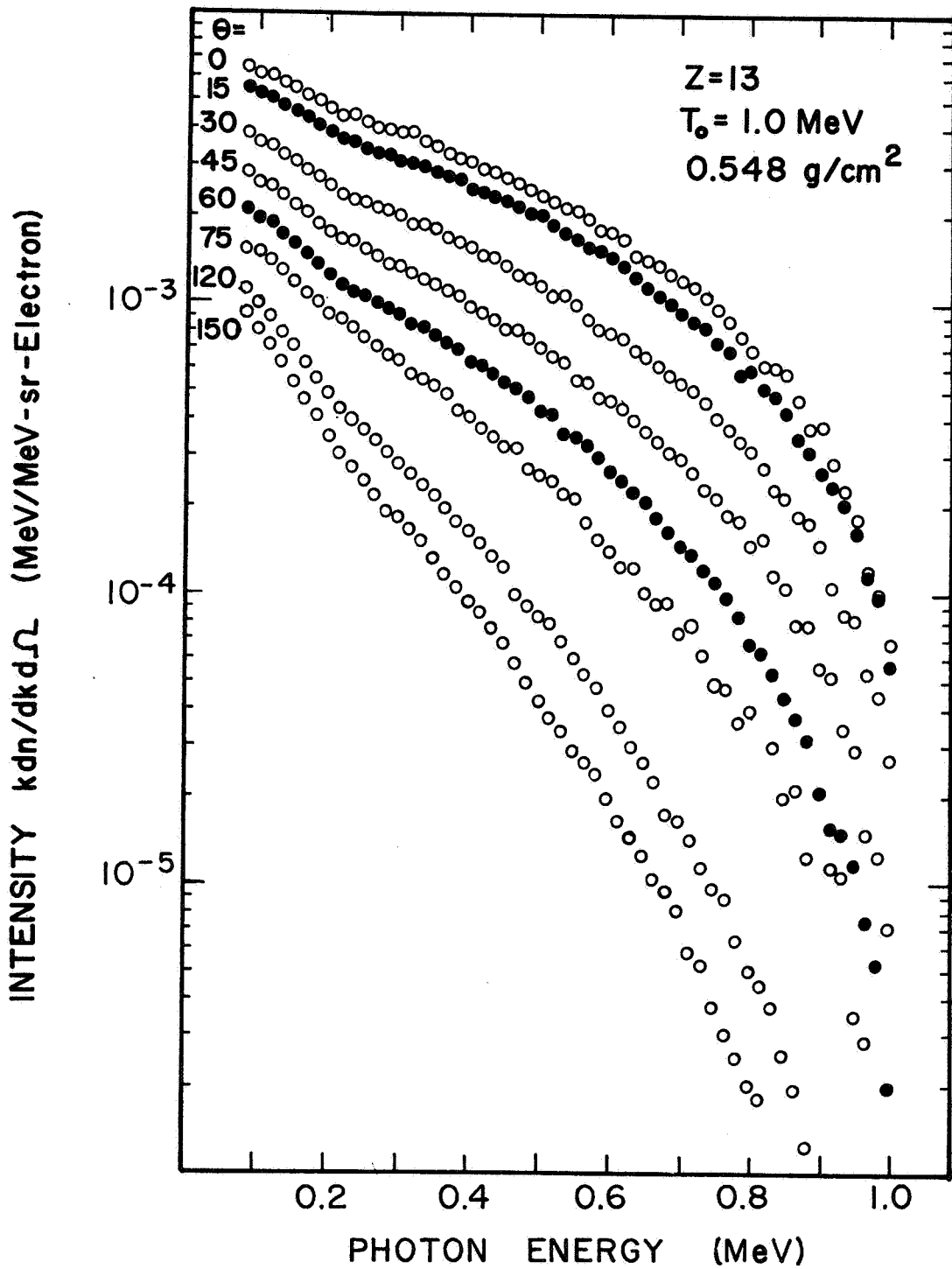
FIGURE 9.   BREMSSTRAHLUNG DIFFERENTIAL INTENSITY SPECTRA FOR 1.0 MeV
ELECTRONS ON A THICK Al TARGET.
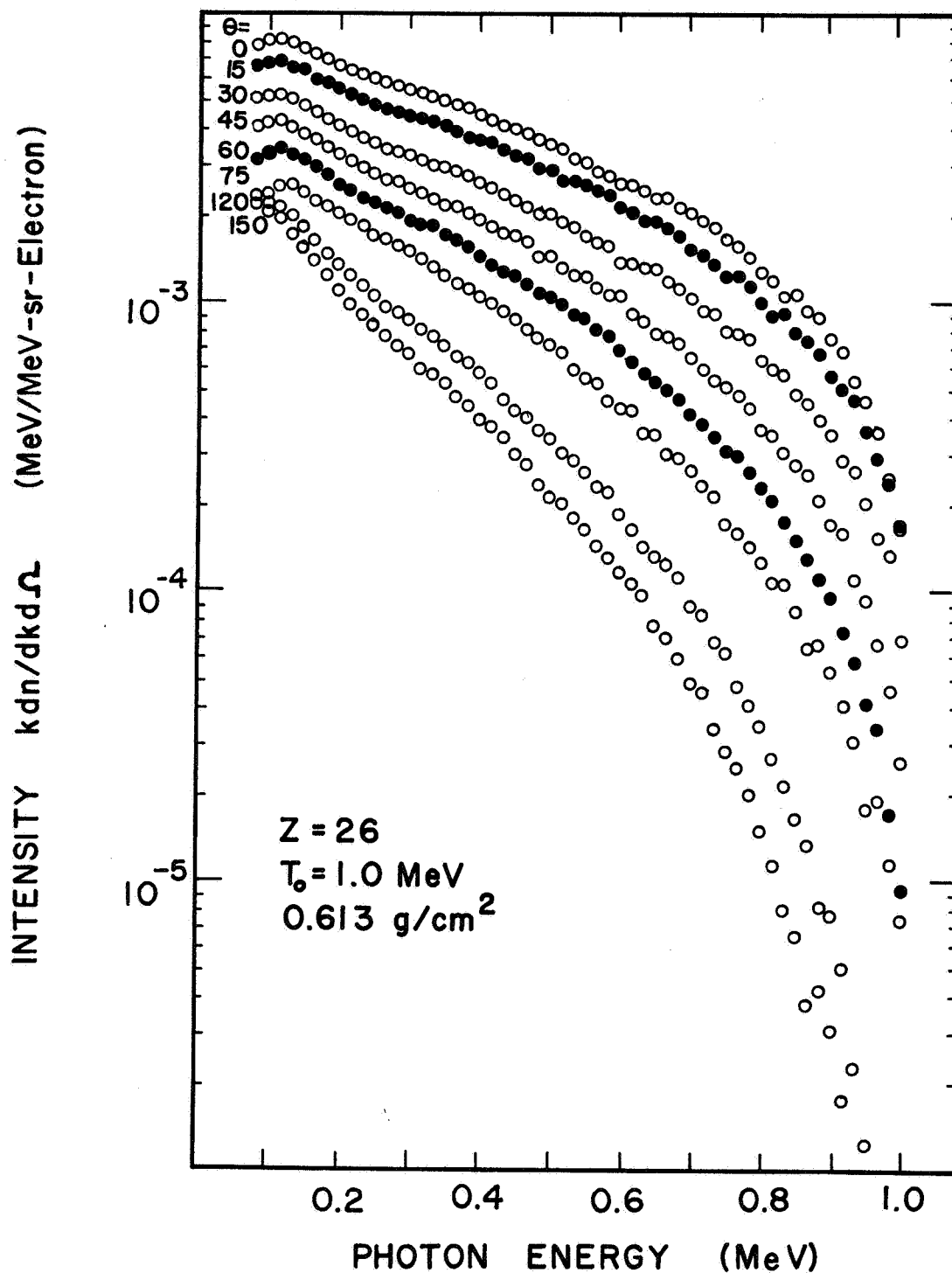
FIGURE 10. BREMSSTRAHLUNG DIFFERENTIAL INTENSITY SPECTRA FOR 1.0 MeV
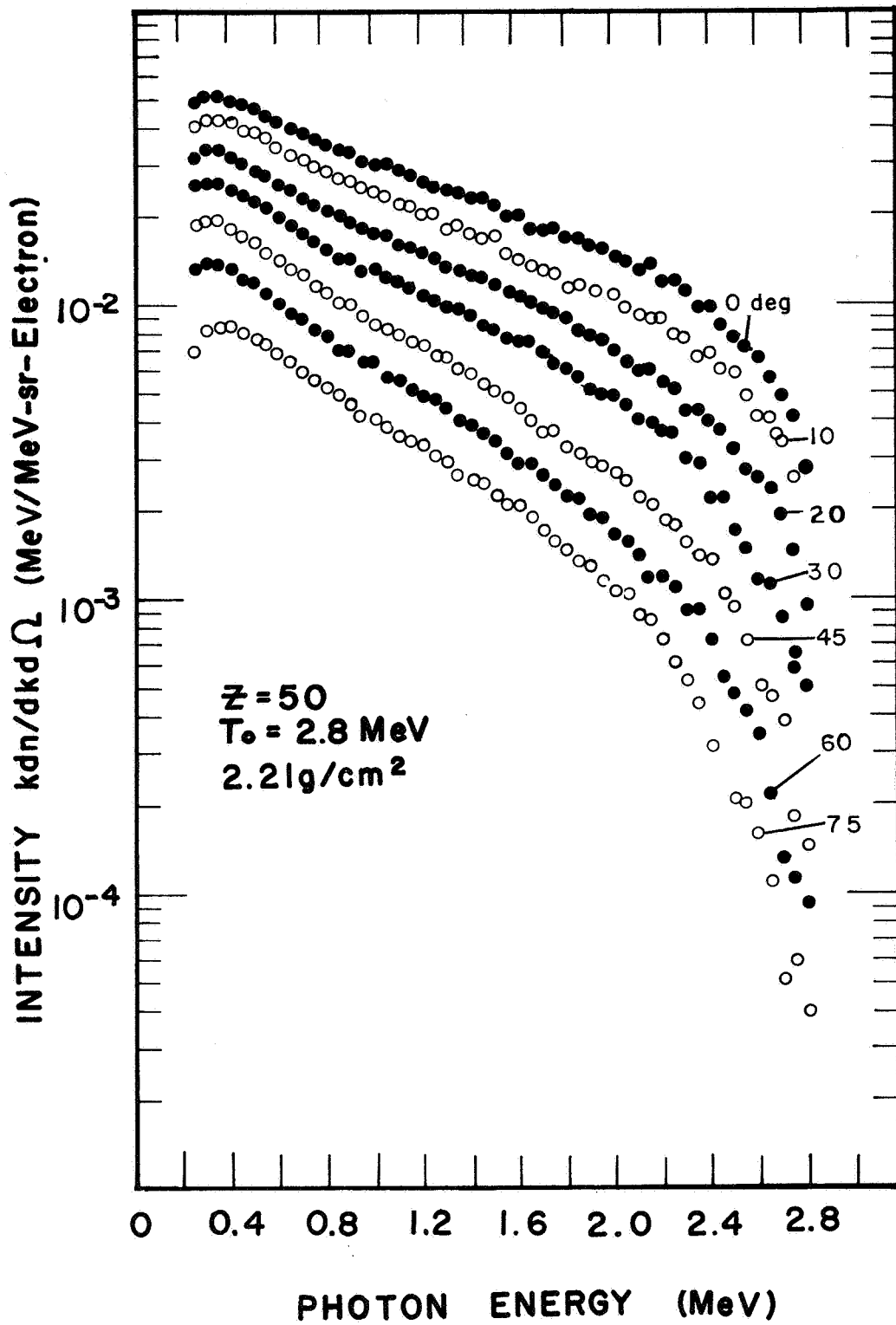ELECTRONS ON A THICK Fe TARGET.
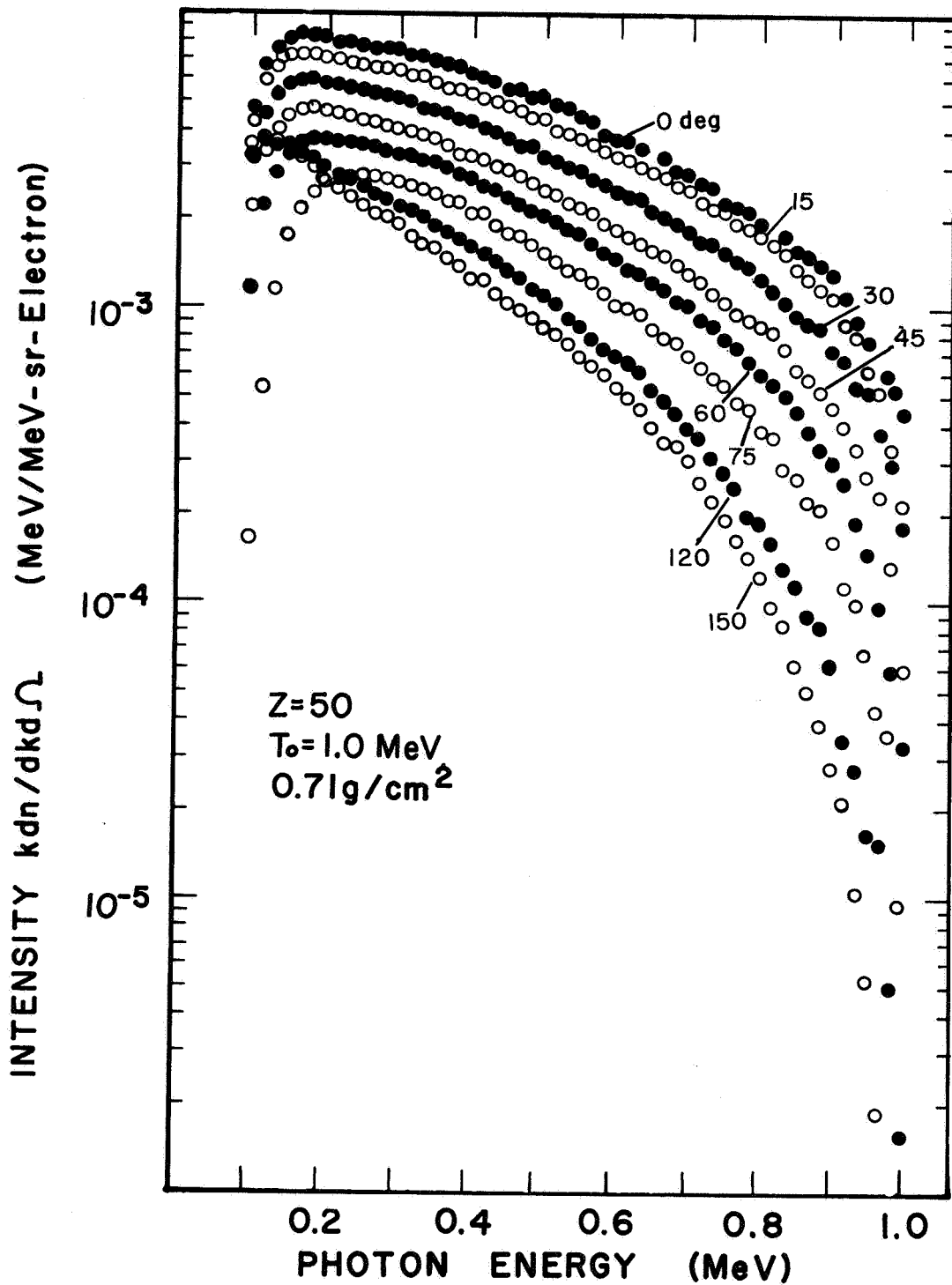
FIGURE 11. BREMSSTRAHLUNG DIFFERENTIAL INTENSITY SPECTRA FOR 1.0 MeV
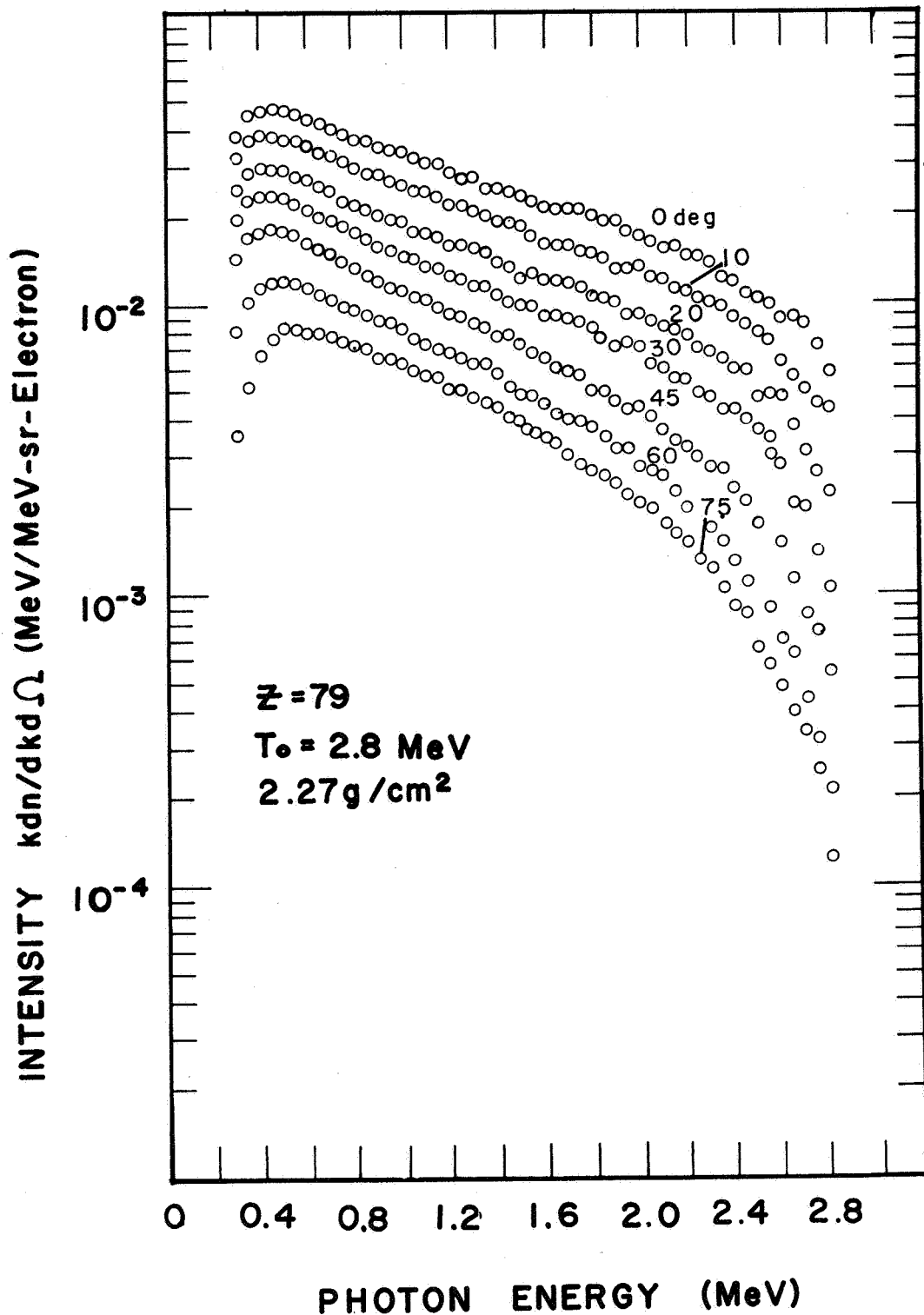ELECTRONS ON A THICK Sn TARGET.
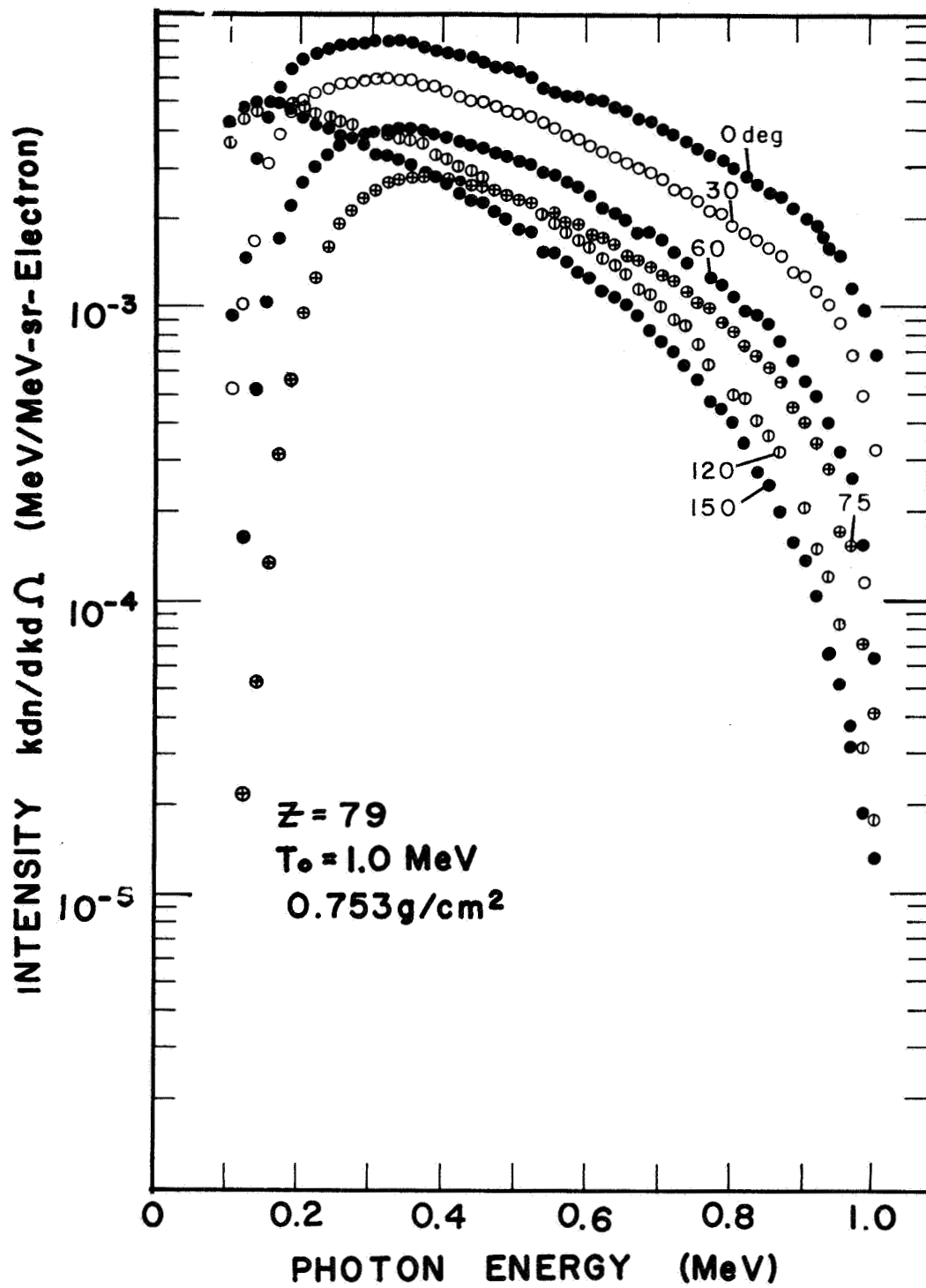
FIGURE 12. BREMSSTRAHLUNG DIFFERENTIAL INTENSITY SPECTRA FOR 1.0 MeV ELECTRONS ON A THICK Au TARGET.
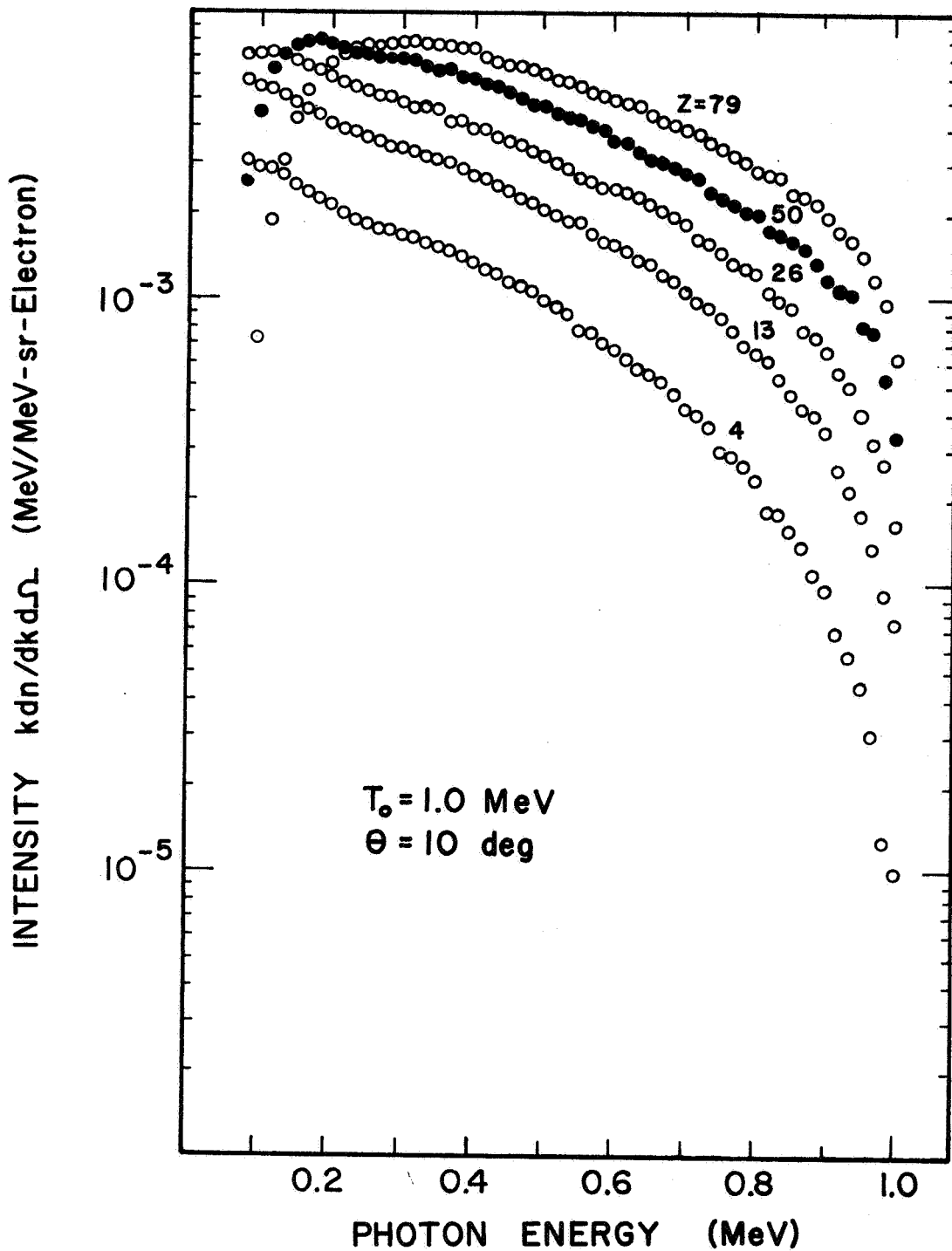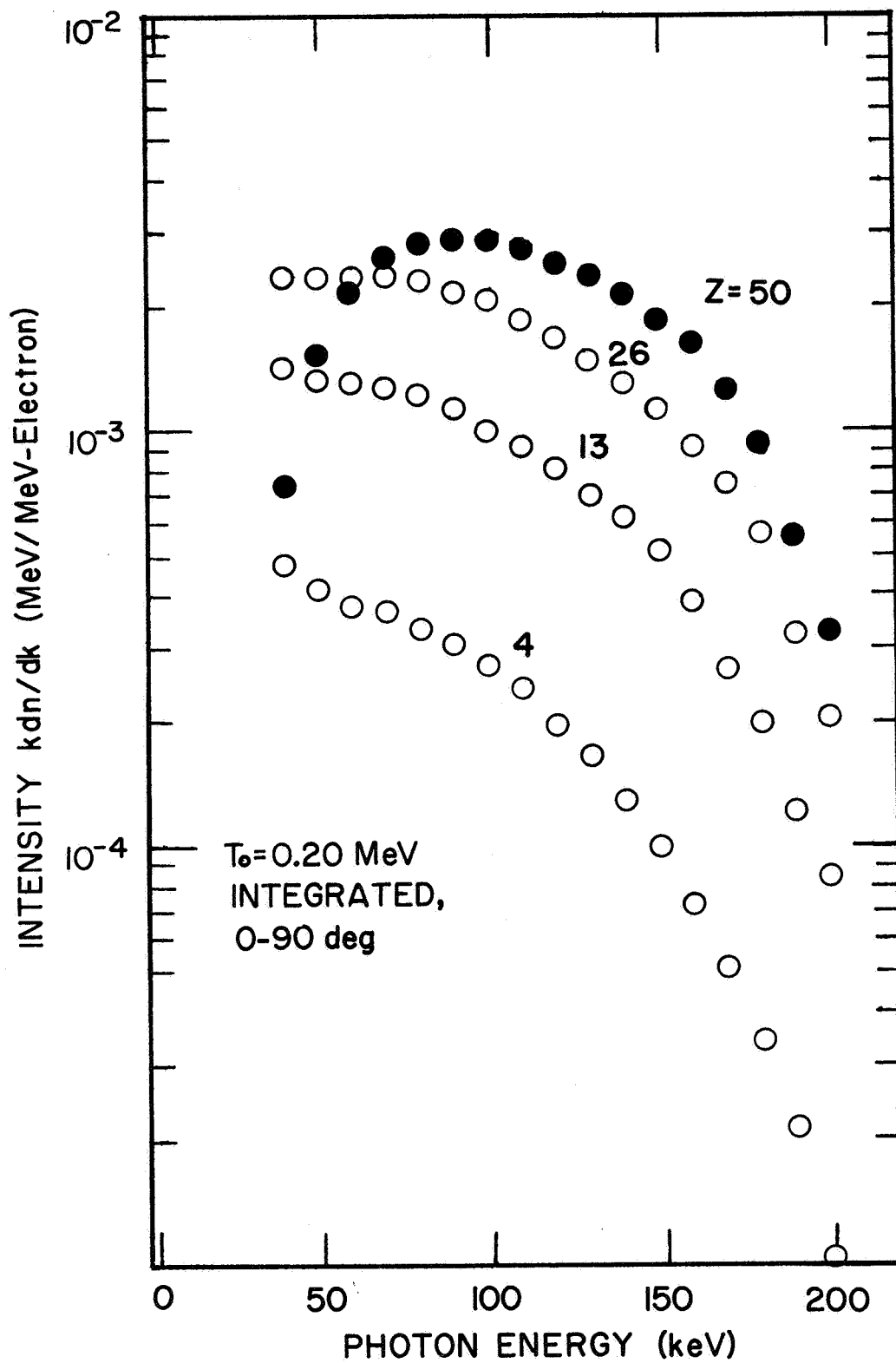
FIGURE 13. BREMSSTRAHLUNG DIFFERENTIAL INTENSITY SPECTRA AT Θ = 10 DEG, FOR 1.0 MeV ELECTRONS ON THICK TARGETS OF Be, Al, Fe, Sn, AND Au.
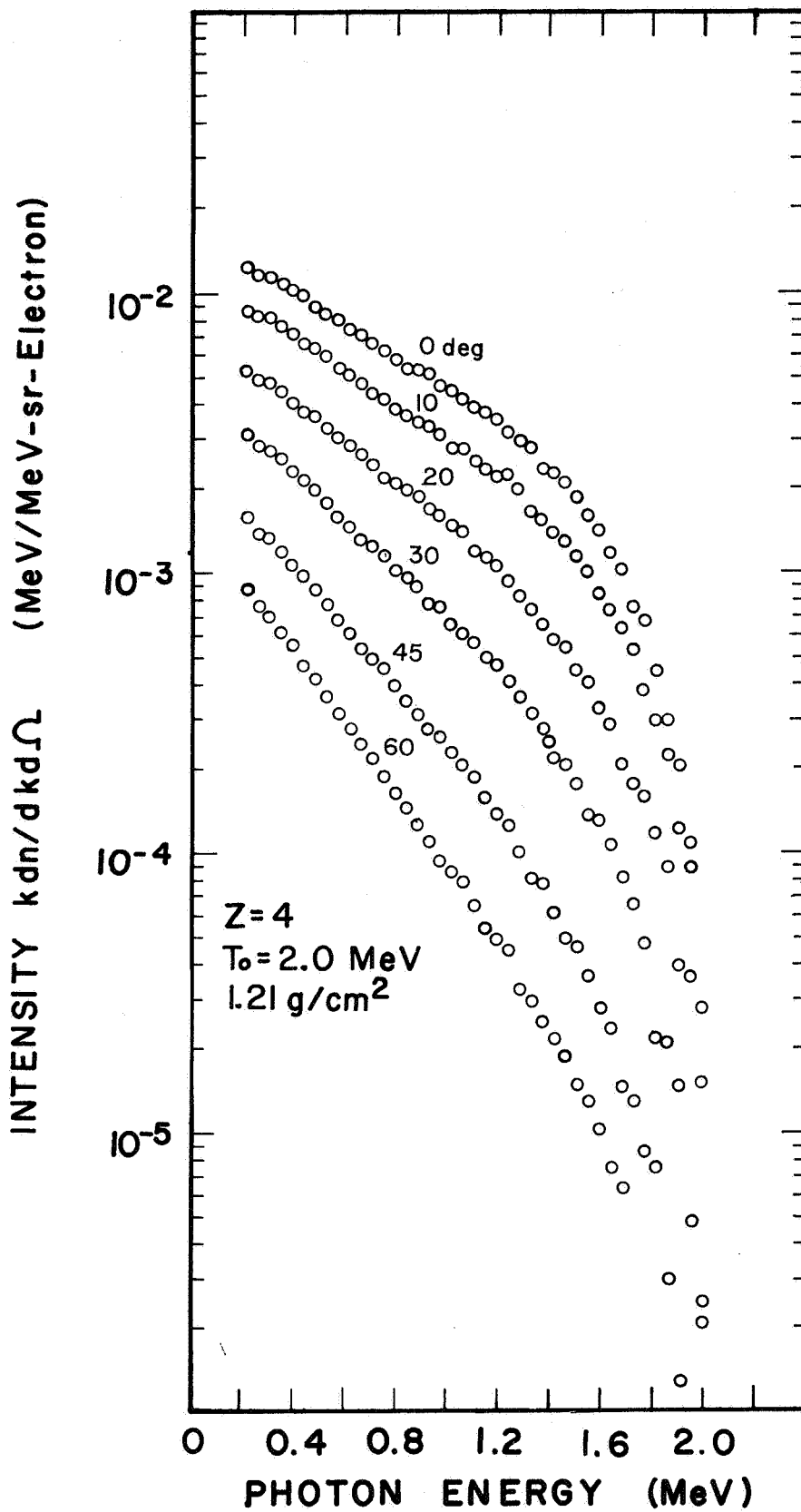
FIGURE 14.   BREMSSTRAHLUNG DIFFERENTIAL INTENSITY SPECTRA FOR 2.0 MeV
ELECTRONS ON A THICK Be TARGET.
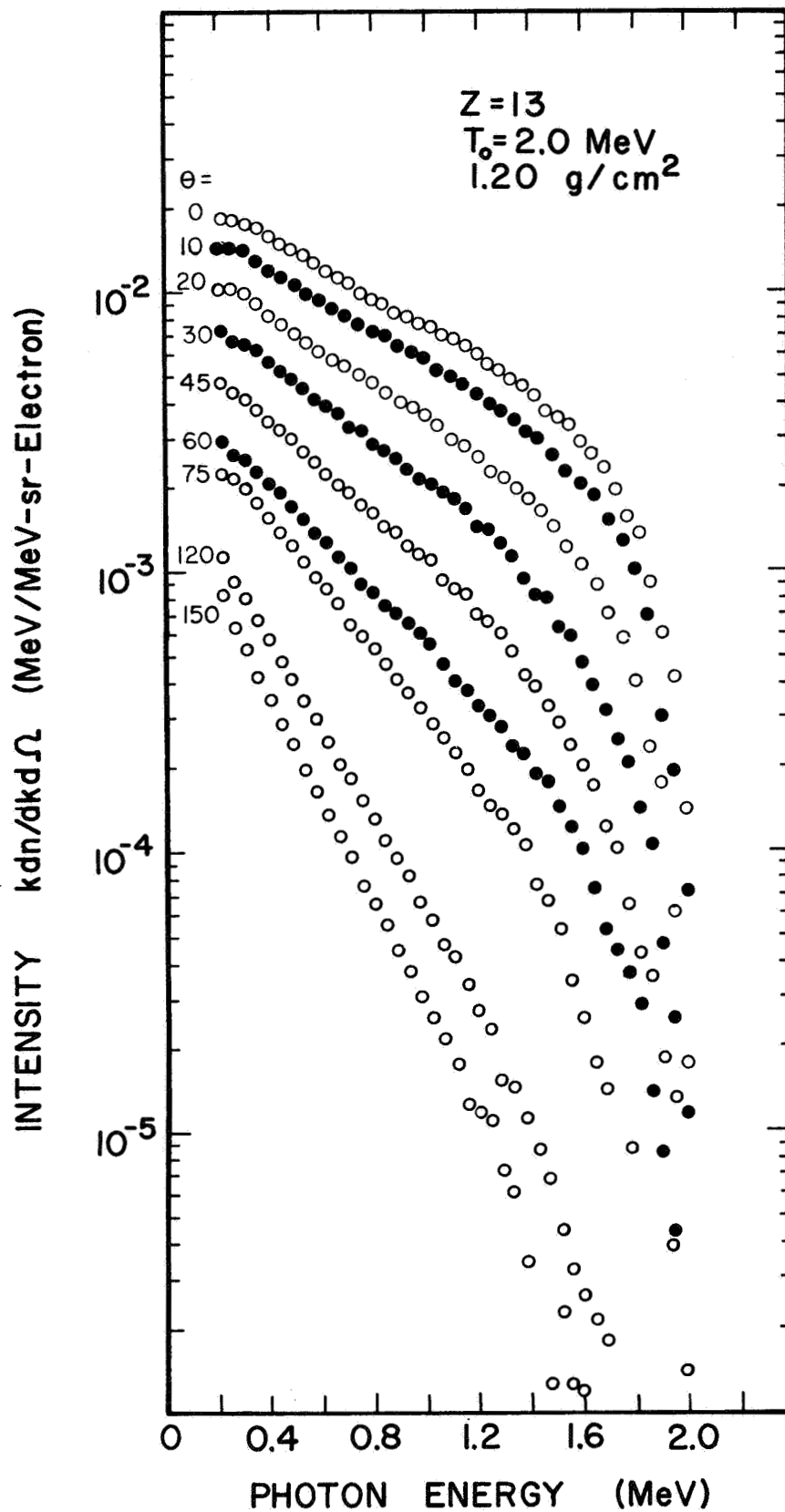
FIGURE 15. BREMSSTRAHLUNG DIFFERENTIAL INTENSITY SPECTRA FOR 2.0 MeV
ELECTRONS ON A THICK Al TARGET.

FIGURE 16. BREMSSTRAHLUNG DIFFERENTIAL INTENSITY SPECTRA FOR 2.0 MeV
ELECTRONS ON A THICK Fe TARGET.

INTENSITY $k\frac{dn}{dk\,d\Omega}$ (MeV/MeV-sr-Electron)

10^{-2}

10^{-3}

10^{-4}

10^{-5}

0 deg
10
20
30
45
60
75
120
150

Z=50
T_o=2.0 MeV
1.47 g/cm^2

0   0.4   0.8   1.2   1.6   2.0

PHOTON ENERGY (MeV)

FIGURE 17.   BREMSSTRAHLUNG DIFFERENTIAL INTENSITY SPECTRA FOR 2.0 MeV
ELECTRONS ON A THICK Sn TARGET.

FIGURE 18. BREMSSTRAHLUNG DIFFERENTIAL INTENSITY SPECTRA FOR 2.0 MeV ELECTRONS ON A THICK Au TARGET.

FIGURE 19. BREMSSTRAHLUNG DIFFERENTIAL INTENSITY SPECTRA FOR 2.8 MeV ELECTRONS ON A THICK Al TARGET.

FIGURE 20. BREMSSTRAHLUNG DIFFERENTIAL INTENSITY SPECTRA FOR 2.8 MeV
ELECTRONS ON A THICK Fe TARGET.

FIGURE 21. BREMSSTRAHLUNG DIFFERENTIAL INTENSITY SPECTRA FOR 2.8 MeV ELECTRONS ON A THICK Sn TARGET.

FIGURE 22. BREMSSTRAHLUNG DIFFERENTIAL INTENSITY SPECTRA FOR 2.8 MeV ELECTRONS ON A THICK Au TARGET.

FIGURE 23. BREMSSTRAHLUNG INTENSITY SPECTRA, INTEGRATED OVER THE FORWARD ANGLES 0 - 90 DEG FOR 0.2 MeV ELECTRONS ON THICK TARGETS OF Be, Al, Fe, and Sn.
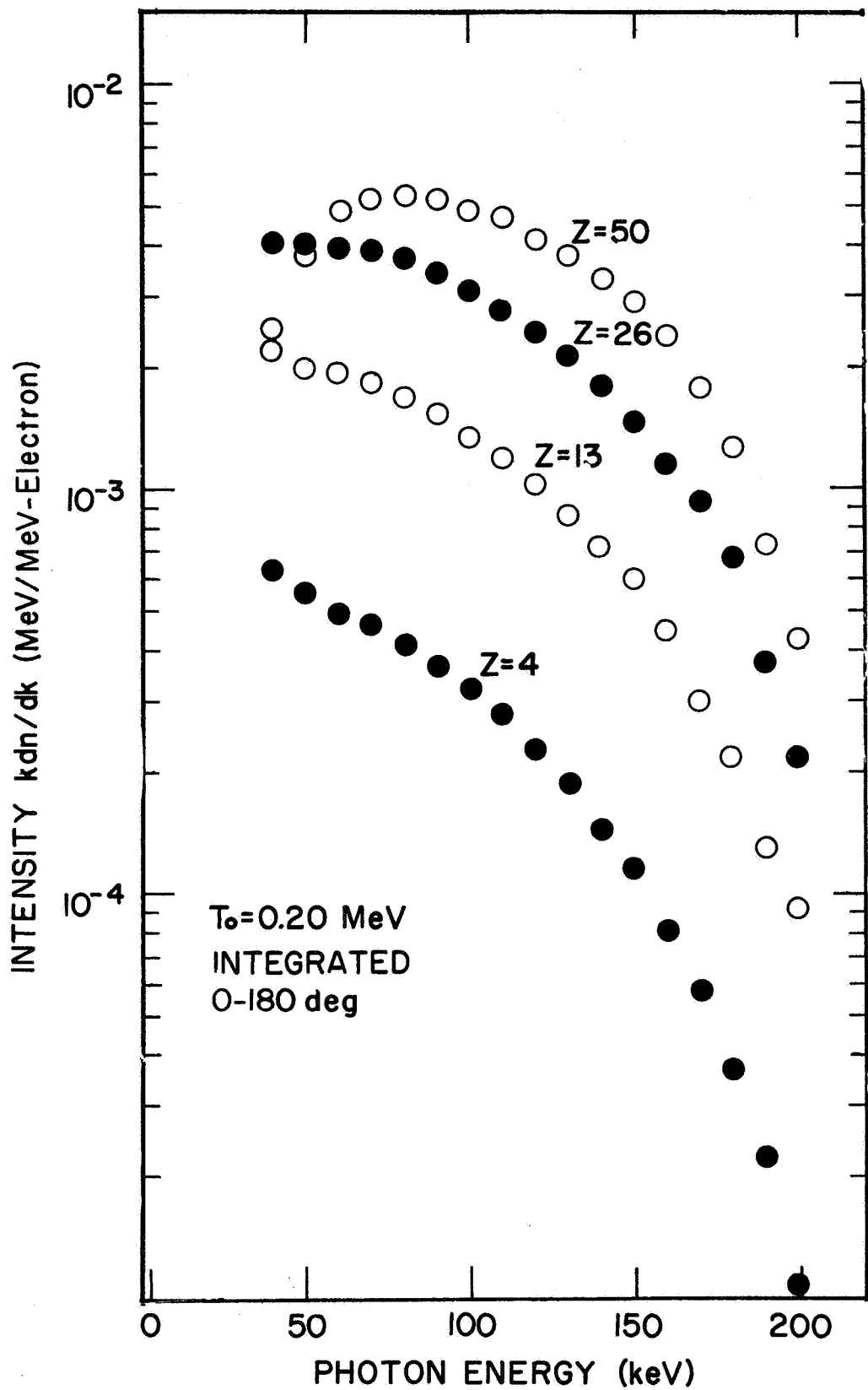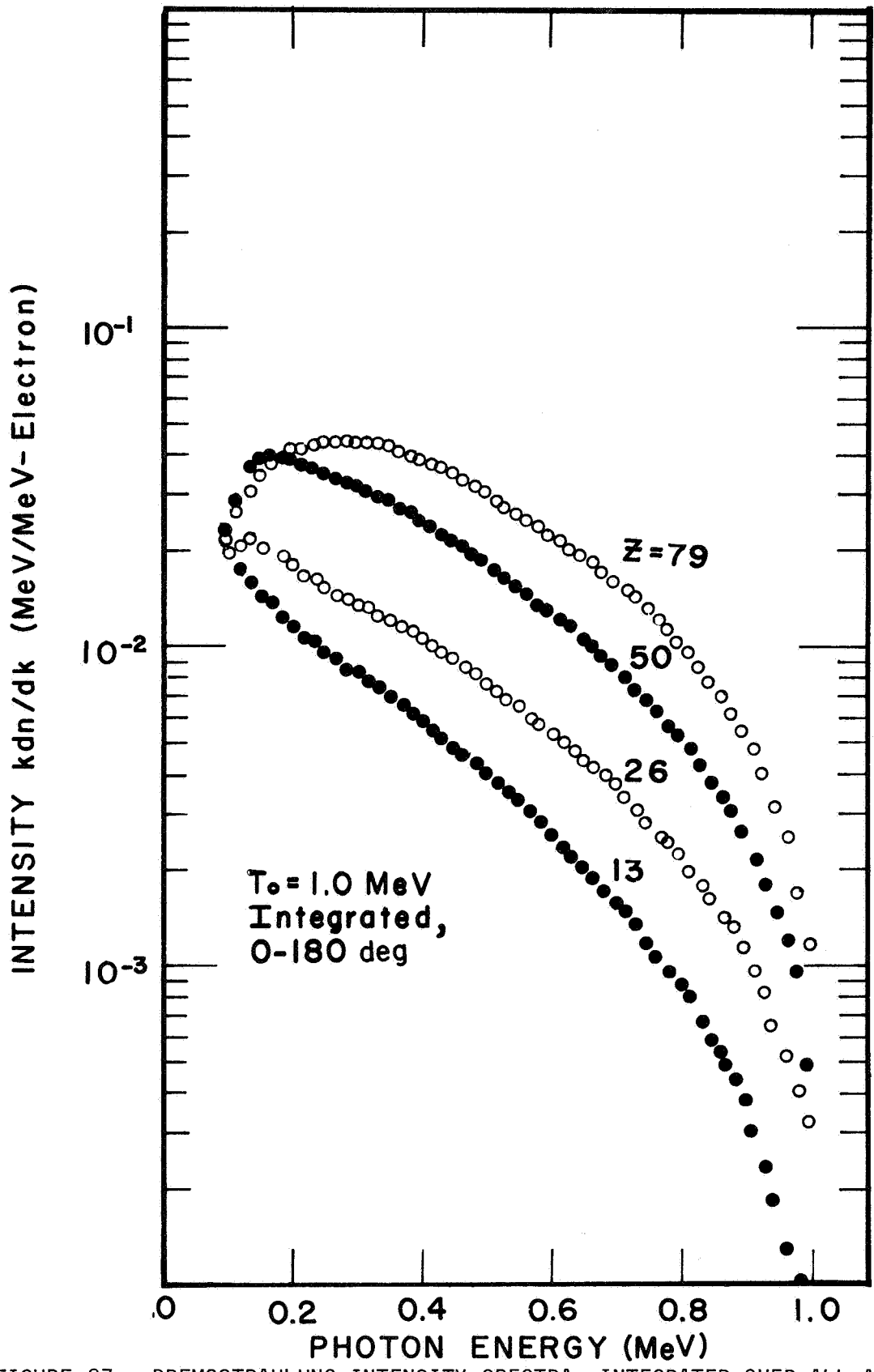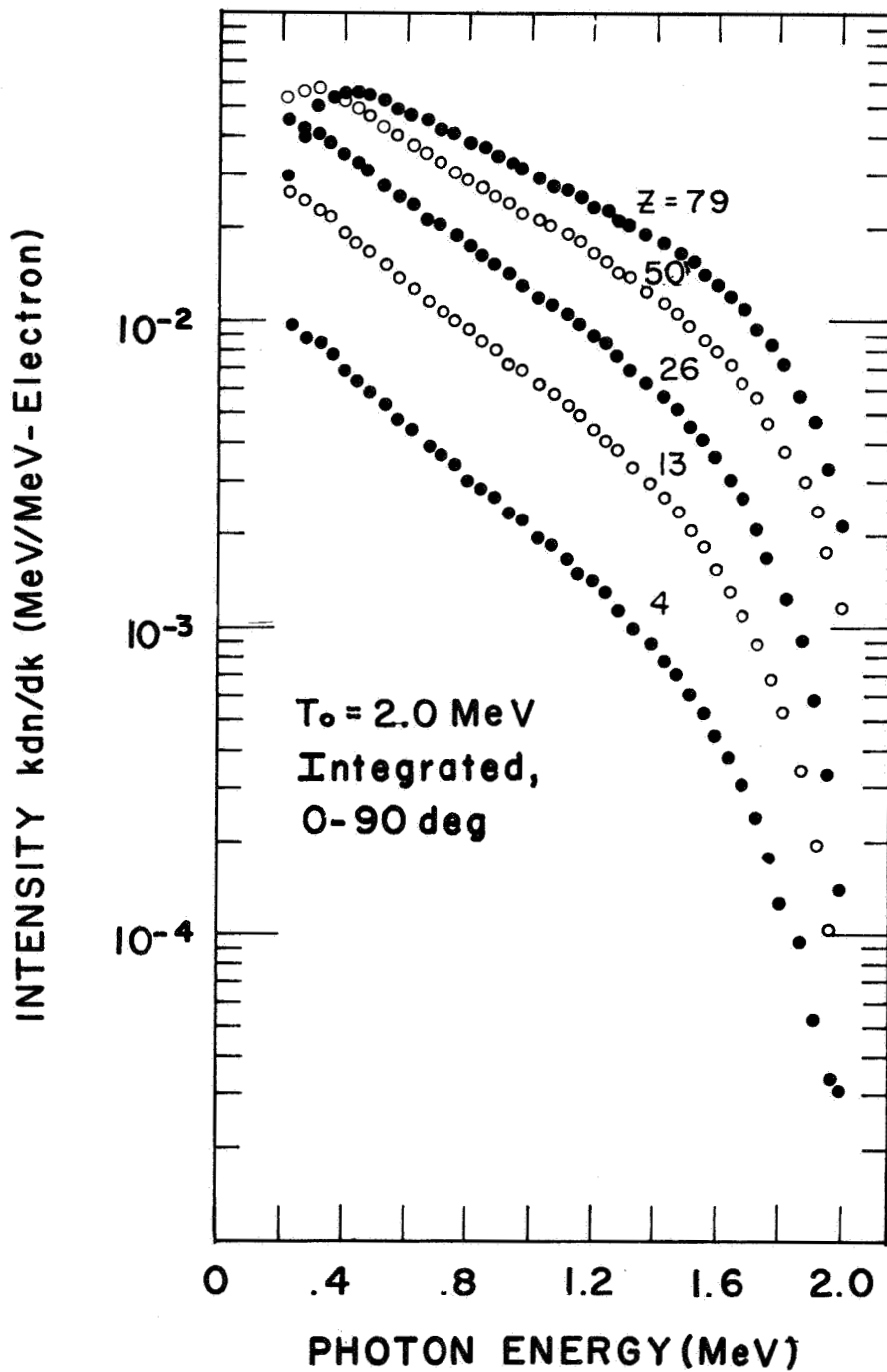
FIGURE 24. BREMSSTRAHLUNG INTENSITY SPECTRA, INTEGRATED OVER ALL ANGLES 0-180 DEG FOR 0.2 MeV ELECTRONS ON THICK TARGETS OF Be, Al, Fe, and Sn.
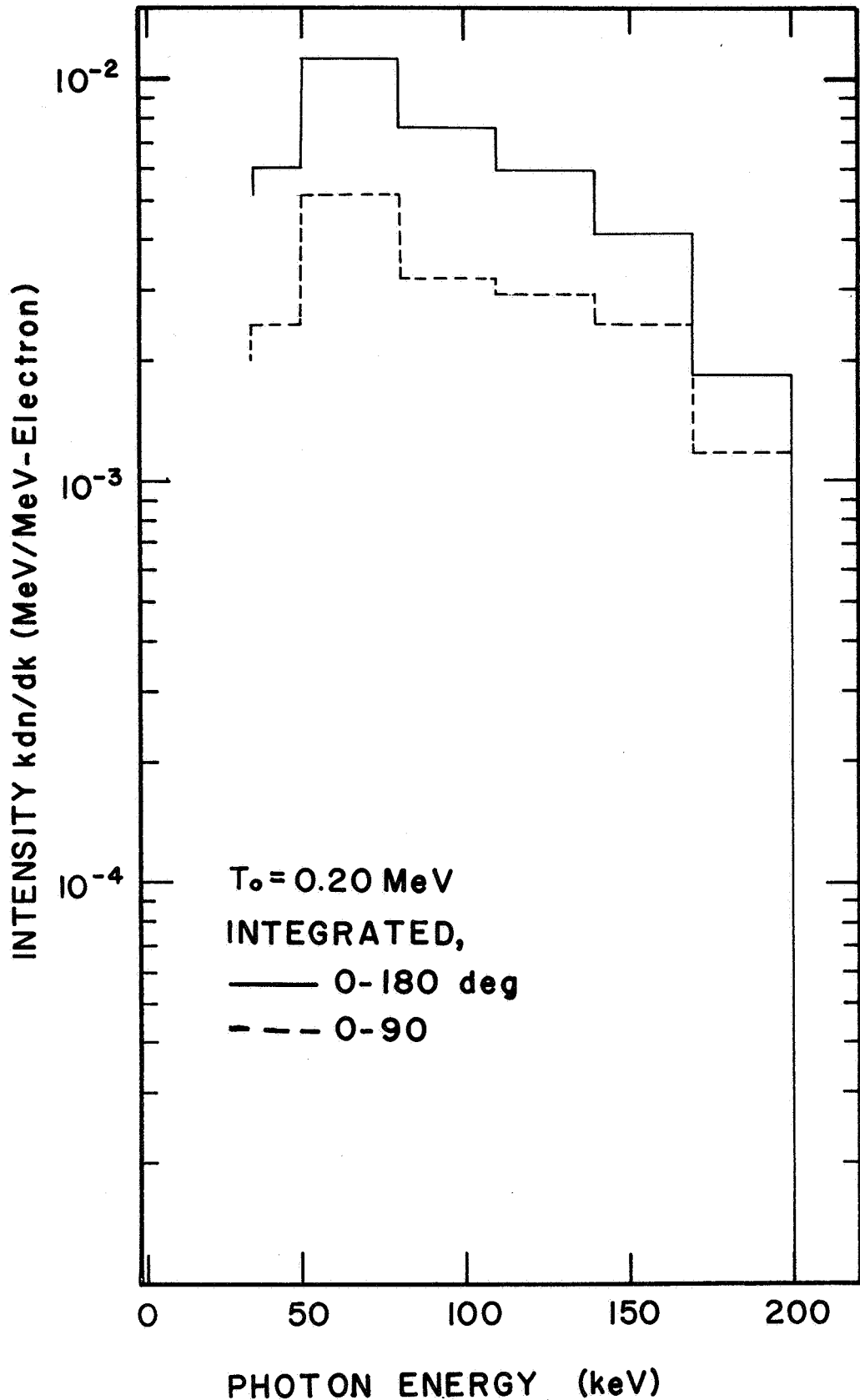
FIGURE 25. BREMSSTRAHLUNG INTENSITY SPECTRA, INTEGRATED OVER ALL
ANGLES 0-180 DEG AND OVER THE FORWARD ANGLES 0-90 DEG
FOR 0.2 MeV ELECTRONS ON A THICK Au TARGET.
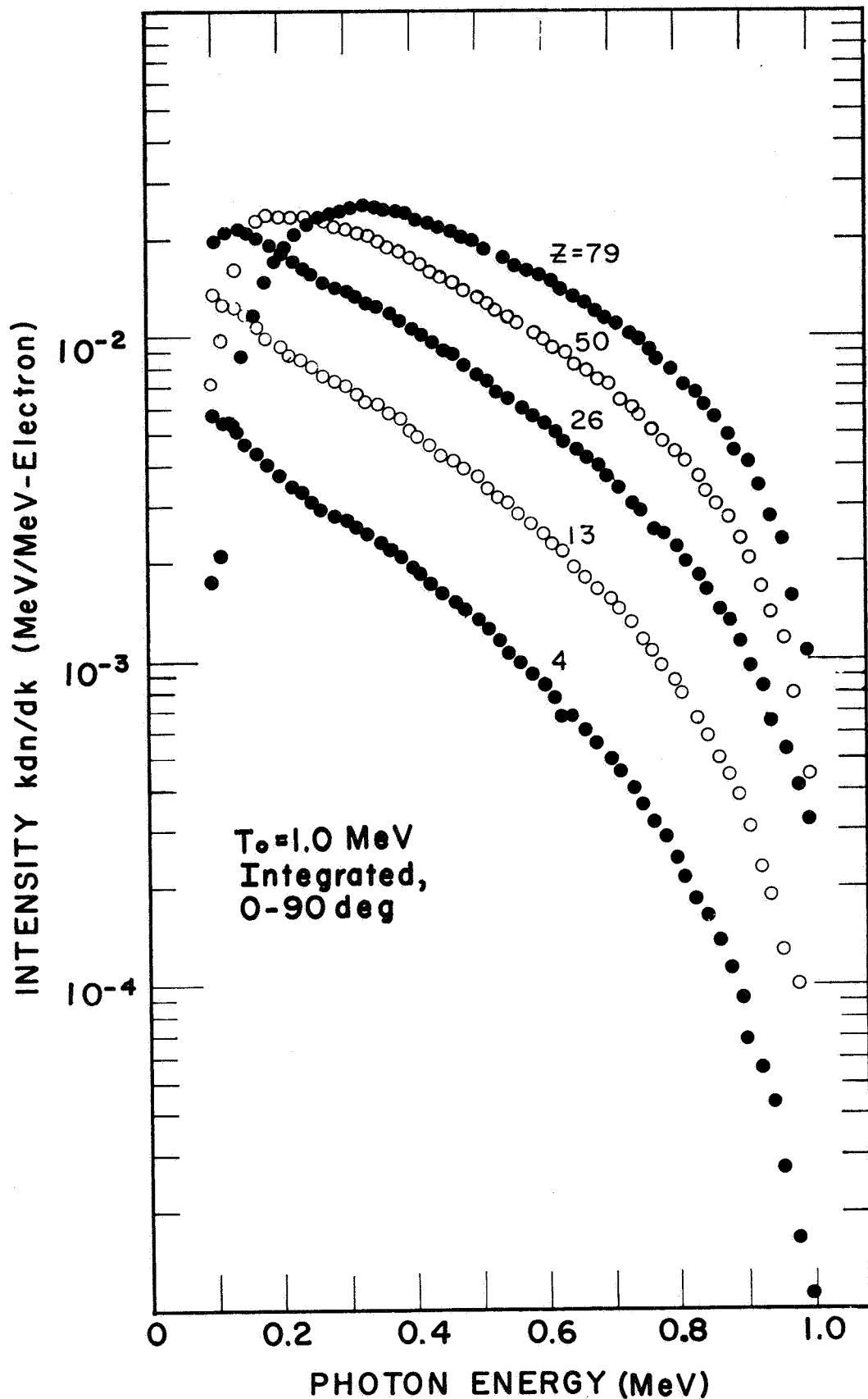
FIGURE 26. BREMSSTRAHLUNG INTENSITY SPECTRA, INTEGRATED OVER THE FORWARD ANGLES 0 - 90 DEG FOR 1.0 MeV ELECTRONS ON THICK TARGETS OF Be, Al, Fe, Sn, AND Au.
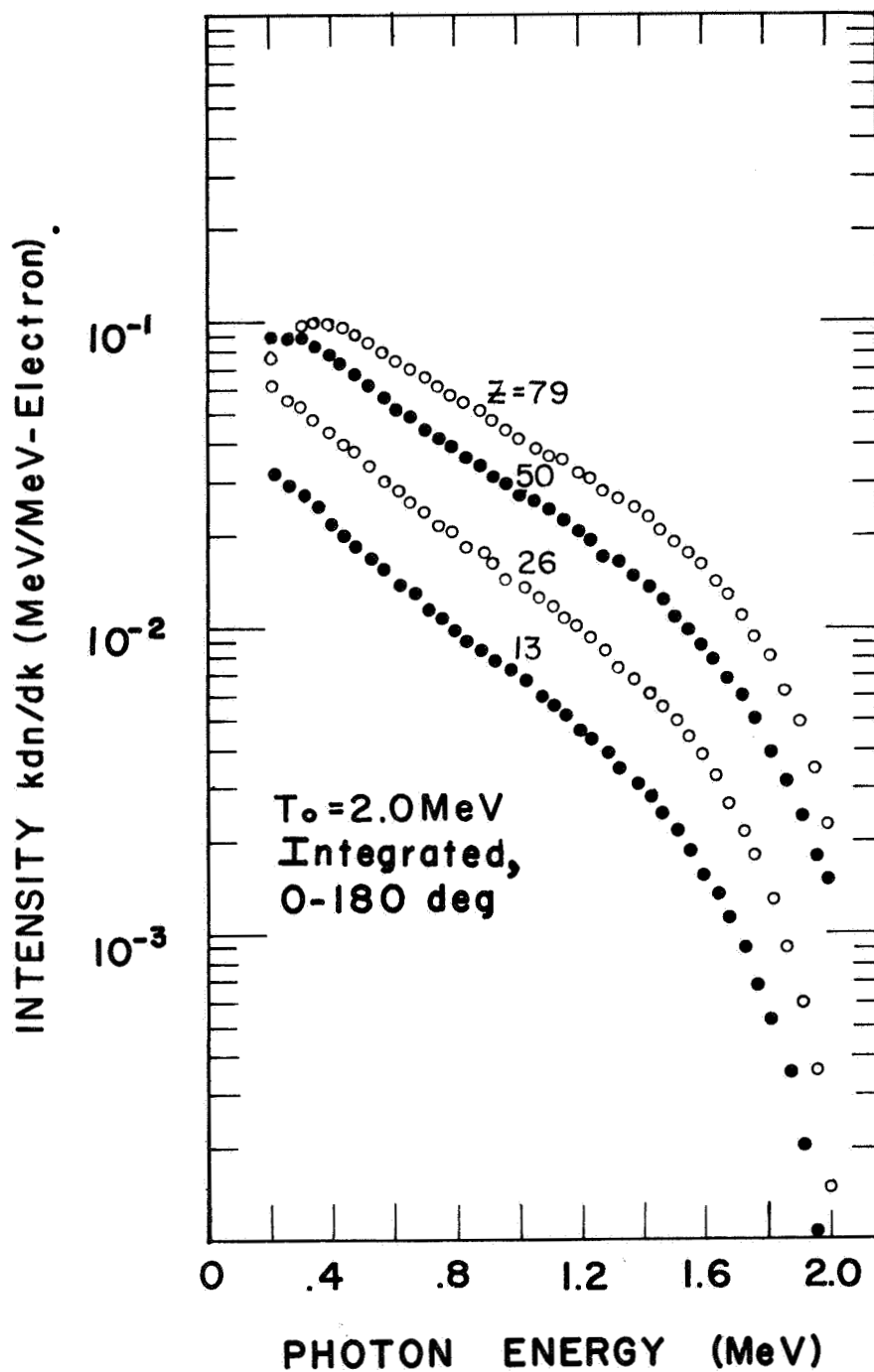
FIGURE 27. BREMSSTRAHLUNG INTENSITY SPECTRA, INTEGRATED OVER ALL ANGLES 0 - 180 DEG FOR 1.0 MeV ELECTRONS ON THICK TARGETS OF Al, Fe, Sn, AND Au.
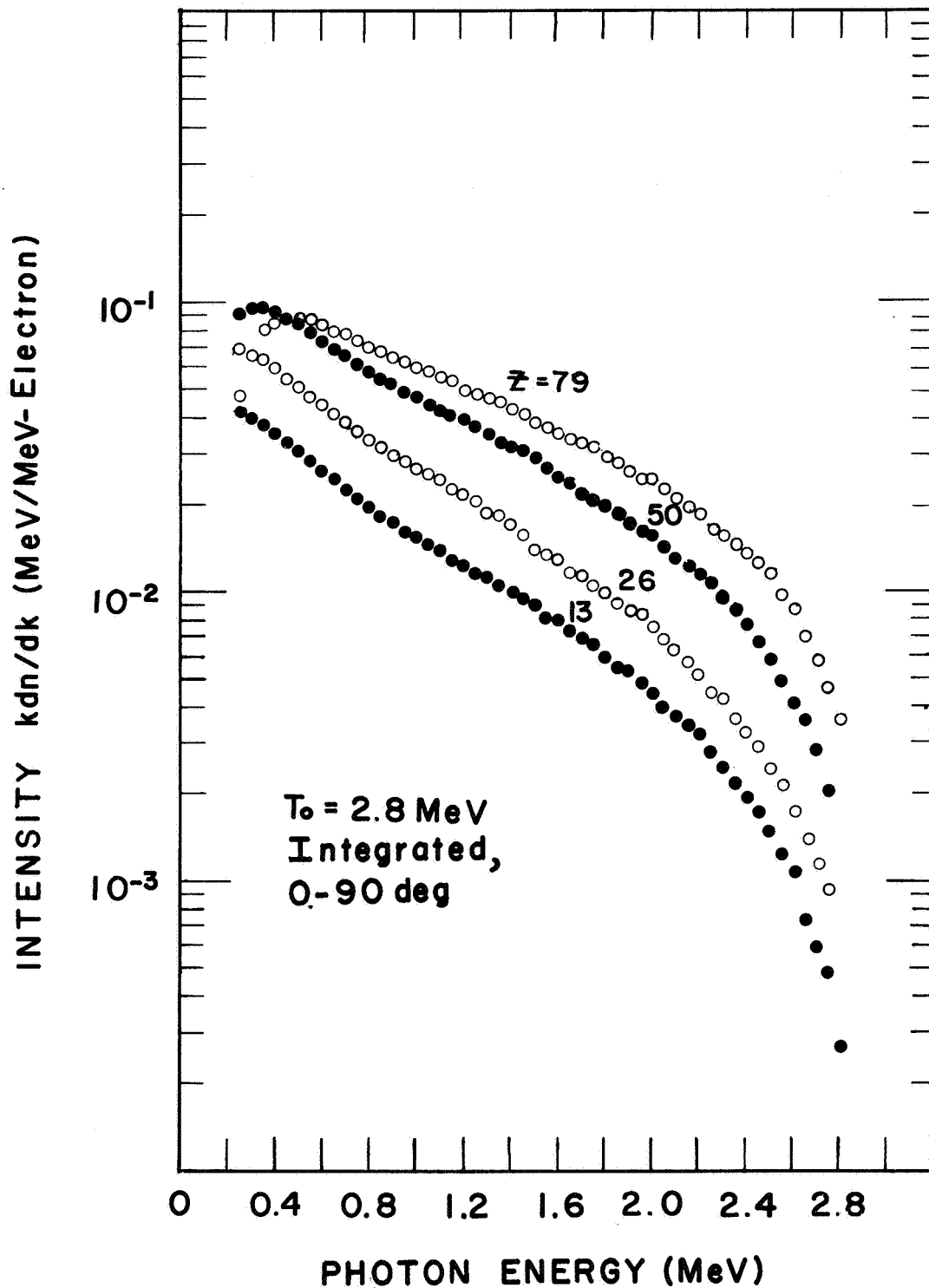
FIGURE 28. BREMSSTRAHLUNG INTENSITY SPECTRA, INTEGRATED OVER THE FORWARD ANGLES 0 - 90 DEG FOR 2.0 MeV ELECTRONS ON THICK TARGETS OF Be, Al, Fe, Sn, AND Au.
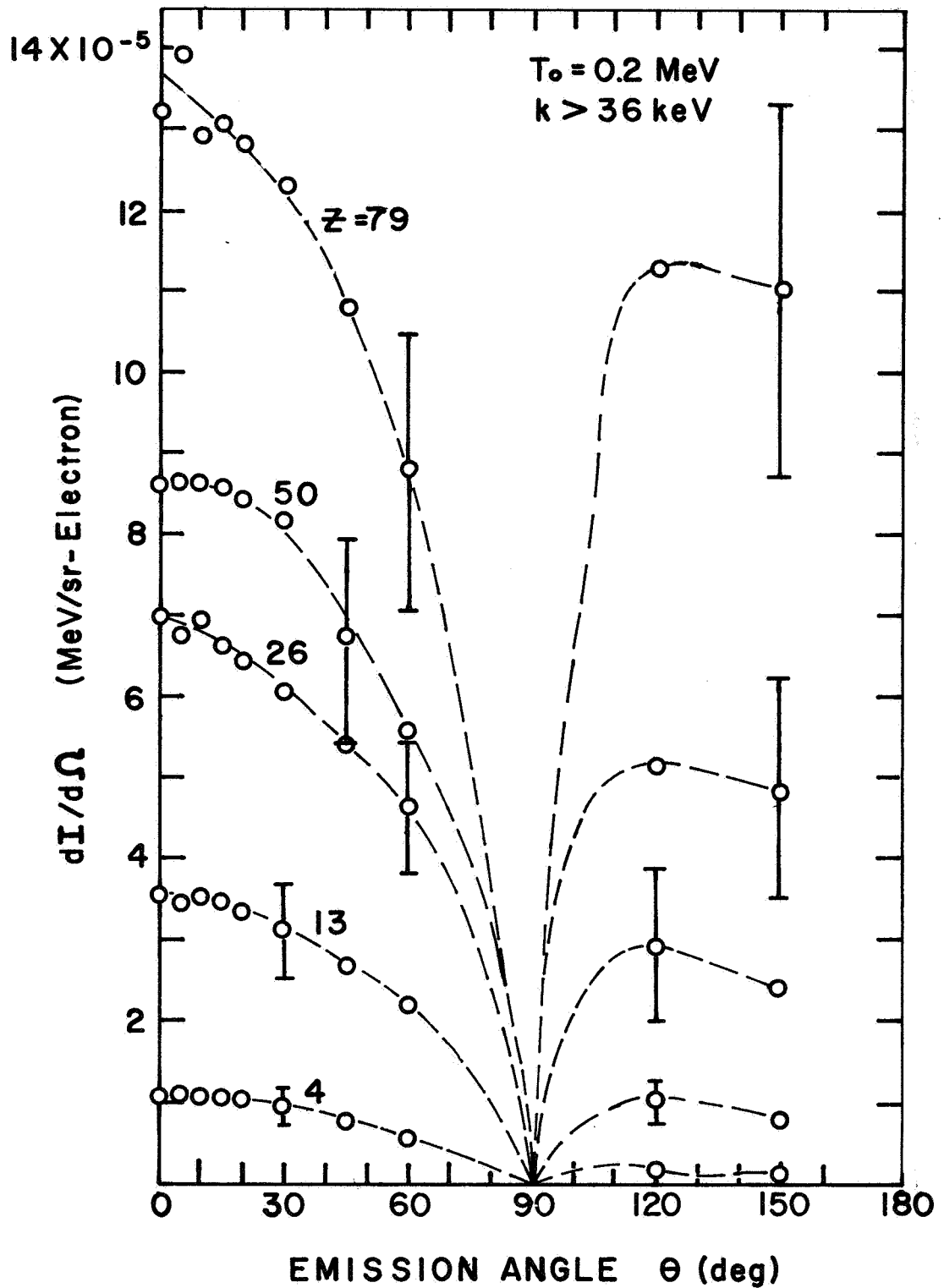
FIGURE 29. BREMSSTRAHLUNG INTENSITY SPECTRA, INTEGRATED OVER ALL ANGLES 0 - 180 DEG FOR 2.0 MeV ELECTRONS ON THICK TARGETS OF Al, Fe, Sn, AND Au.

FIGURE 30. BREMSSTRAHLUNG INTENSITY SPECTRA, INTEGRATED OVER THE FORWARD ANGLES 0 – 90 DEG FOR 2.8 MeV ELECTRONS ON THICK TARGETS OF Al, Fe, Sn, AND Au.
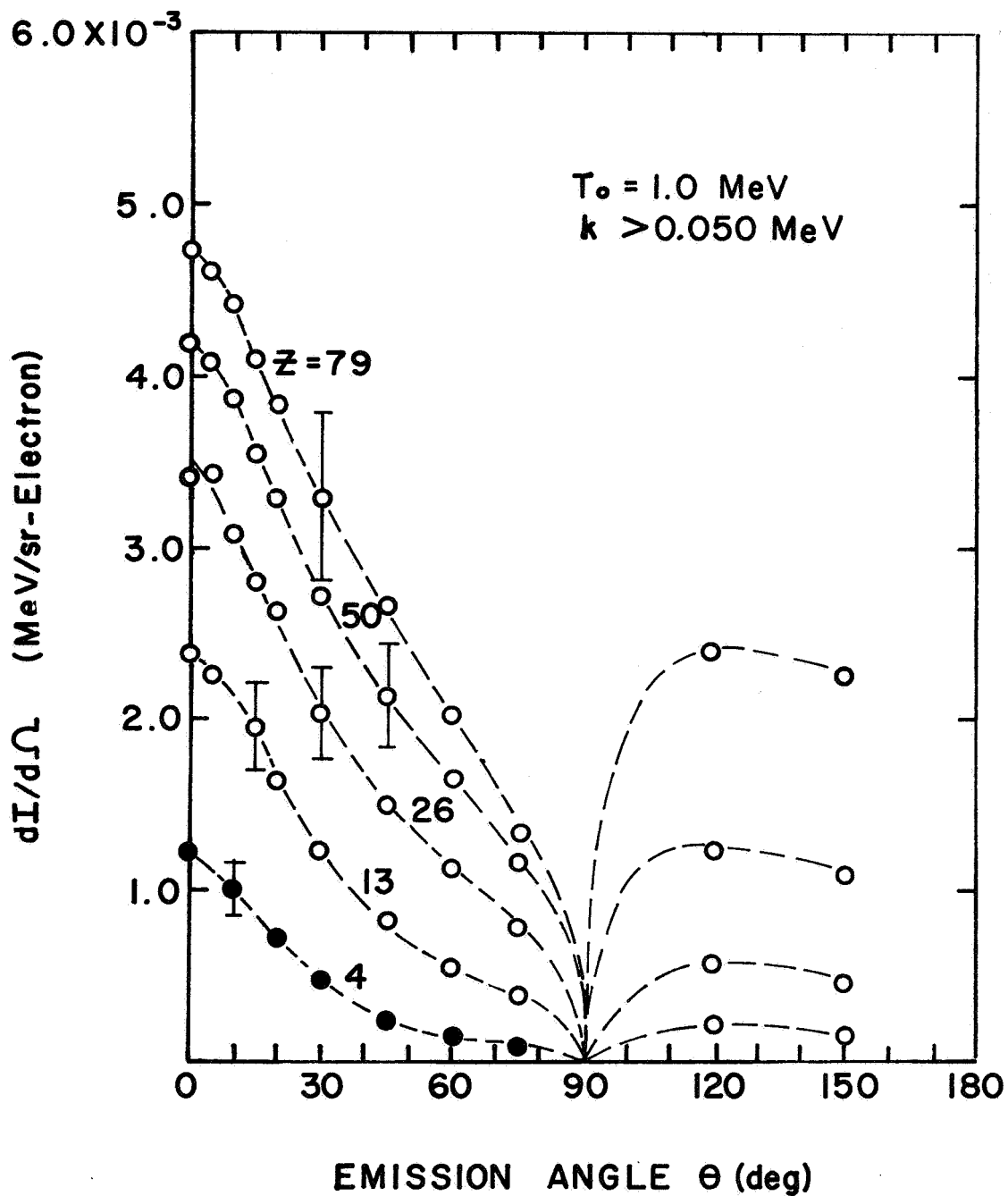
FIGURE 31. ANGULAR DISTRIBUTIONS OF BREMSSTRAHLUNG INTENSITIES, INTEGRATED OVER PHOTON ENERGY, k > 0.036 MeV, FOR 0.2 MeV ELECTRONS ON THICK TARGETS OF Be, Al, Fe, Sn, AND Au.

FIGURE 32. ANGULAR DISTRIBUTIONS OF BREMSSTRAHLUNG INTENSITIES, INTEGRATED OVER PHOTON ENERGY, k > 0.050 MeV, FOR 1.0 MeV ELECTRONS ON THICK TARGETS OF Be, Al, Fe, Sn, AND Au.
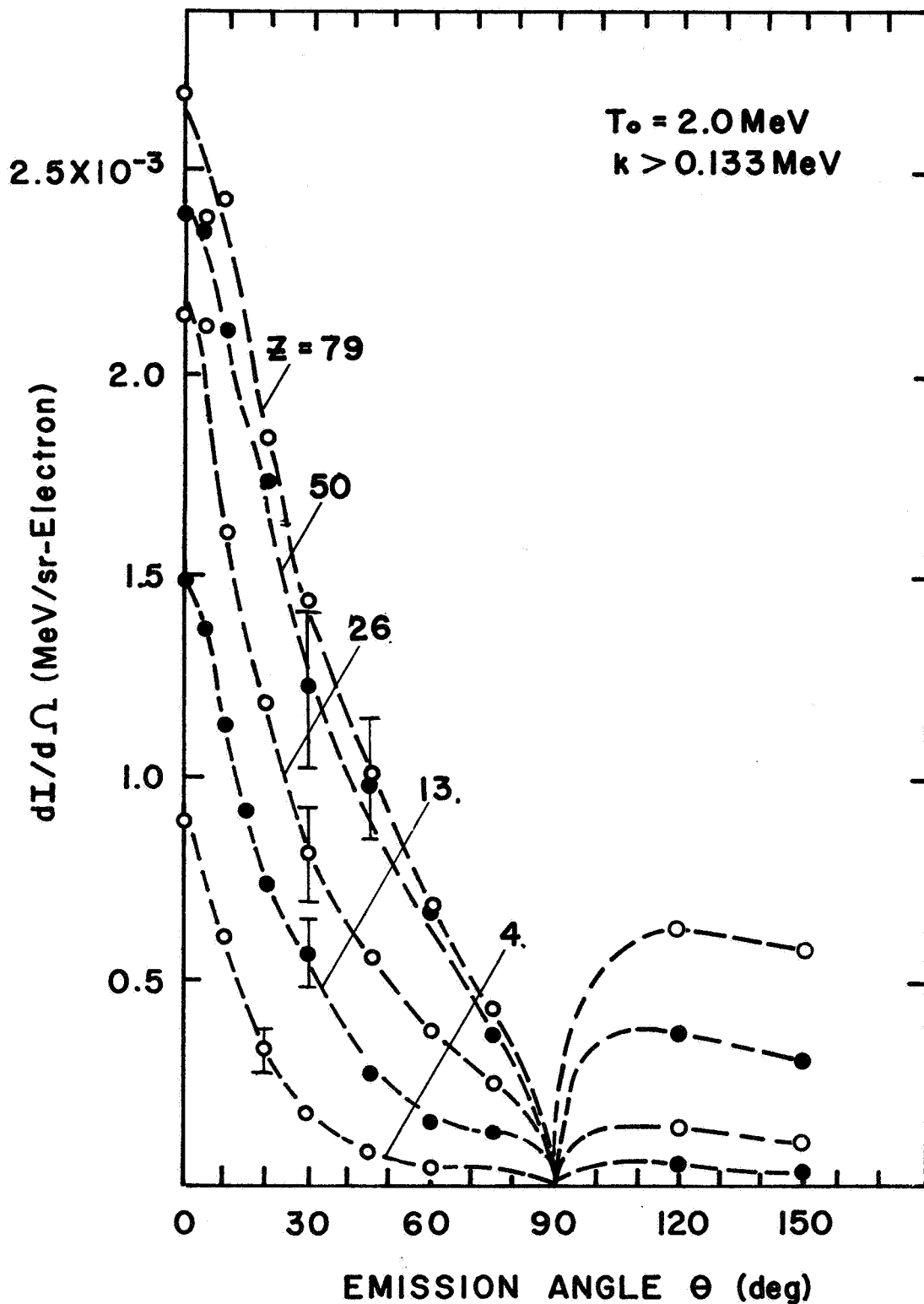
FIGURE 33. ANGULAR DISTRIBUTIONS OF BREMSSTRAHLUNG INTENSITIES, INTEGRATED OVER PHOTON ENERGY, k > 0.133 MeV, FOR 2.0 MeV ELECTRONS ON THICK TARGETS OF Be, Al, Fe, Sn, AND Au.
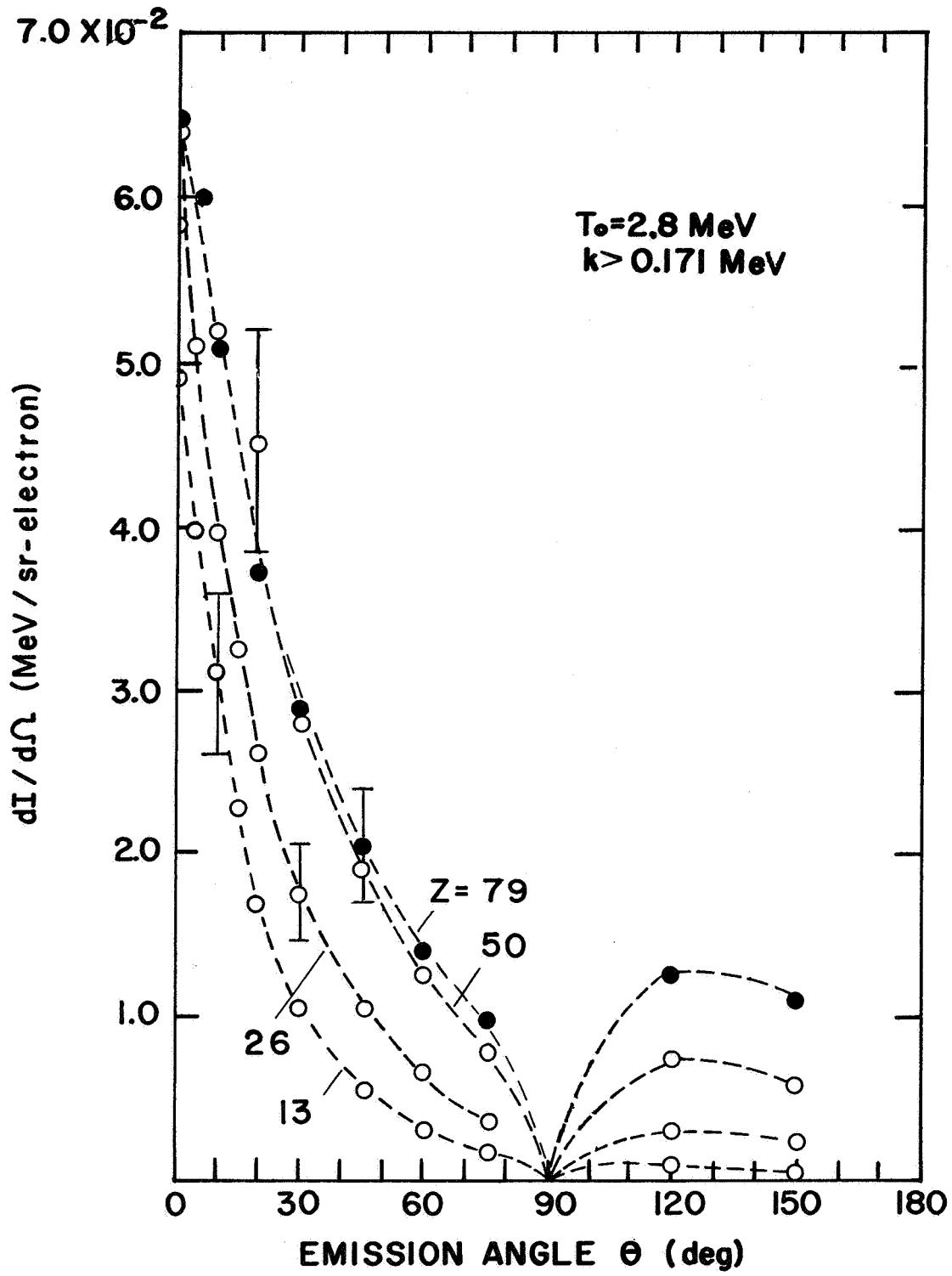
FIGURE 34. ANGULAR DISTRIBUTIONS OF BREMSSTRAHLUNG INTENSITIES, INTEGRATED OVER PHOTON ENERGY, k > 0.171 MeV, FOR 2.8 MeV ELECTRONS ON THICK TARGETS OF Al, Fe, Sn, AND Au.
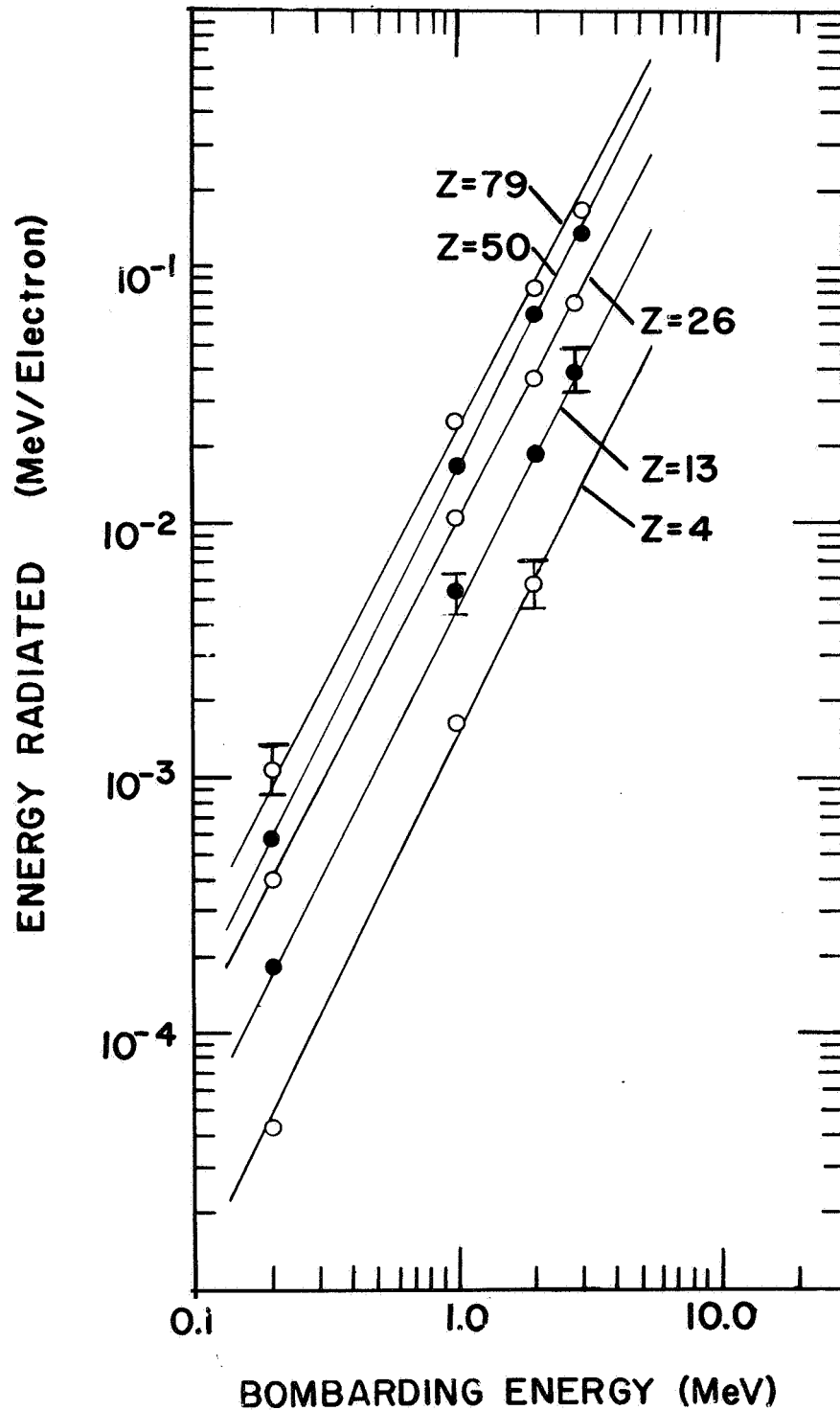
FIGURE 35. ENERGY RADIATED FROM THICK TARGETS OF Be, Al, Fe, Sn, AND Au AS A FUNCTION OF BOMBARDING ENERGY, T_0. THE RESPECTIVE LOWER CUT-OFF PHOTON ENERGIES FOR T_0 = 0.2, 1.0, 2.0, AND 2.8 MeV ARE 36 keV, 50 keV, 133 keV, AND 171 keV.